Design of a High Intensity Ultrasound Dispersion Cell

Clinton Foster

Supervisor: Dr J. Tapson

Co-supervisor: Dr B.J.P. Mortimer

Submitted to the Faculty of Electrical Engineering, University of Cape Town in fulfilment of the requirements for the Degree Masters of Science in Engineering.

Cape Town, November 2002

Acknowledgments

First and foremost, I would like to thank Christ for every good thing given to me. For every honourable, loving and great thing in me, I give praise and credit to Christ Jesus.

I would also like to thank the following people for their help with this project:

Dr. John Tapson for his role in supervising the project, his encouragement and proof reading of this dissertation.

Dr. Bruce Mortimer for his encouragement, interest and advice for the duration of the project.

Mr. Henry Milner for his initiation of the project and his advice on the chemistry involved as well as the loan of valuable equipment.

Mr. Casius Gourgel for his help with testing and excellence in his work.

Mr. Brett Wilson, Mr. Stanley Adams, Mr. Willem Kriege and Mr. Jacque Wheeler for their advice, interest and assistance in numerous areas.

Mrs. Jacki Mun-Gavin for her tireless efforts in proof reading this dissertation, without her assistance this project would not have been completed.

Declaration

The content of this thesis is my own work if not otherwise referenced and has not been submitted for any other academic qualification or examination. The opinions expressed herein are my own and not necessarily that of the University.

Clinton Foster

Synopsis

The aim of this project was to provide detailed research on the factors causing mechanical damage in a high power ultrasound environment, and to give recommendations for the production of an ultrasonic dispersion cell with a removable treatment vessel. The primary mechanism for causing this dispersion was cavitation: a void of air or vapour in a liquid medium that grows and collapses in an intense ultrasonic sound field. The secondary mechanism was a phenomenon called acoustic streaming which provides a macro mixing effect, also caused by intense ultrasound.

Streaming and, even more so, cavitation were difficult to measure and for this reason a refinement of a method to map cavitation fields with aluminium foil was developed. This involved using digital image processing to extract quantitative information from damaged foil samples.

A large portion of the project focused on the overcoming of absorption and subsequent rapid attenuation of sound between the transducer (ultrasonic source) and the treatment vessel. This absorption was due to a number of interrelated factors: reflection of sound at material boundaries; cavitation clouds causing sound scattering; energy absorption; and conventional absorption in liquids due to viscous damping. A number of strategies were employed to overcome this absorption problem: the use of increased static pressure to suppress cavitation in certain areas; the use of multiple transducers; and, as a result, multiple paths for the sound to enter the vessel. A combination of static pressure and multiple transducers were also tested. A number of different media were tested for their ability to transmit sound and an optimum solution was recommended. Streaming and the physical constraints affecting streaming in the treatment vessel were tested to give a practical guide to the factors producing streaming. Then, as the temperature of the liquid affects absorption, cavitation threshold, and the ability of a solvent to dissolve, a look at the thermal aspects of the system was discussed.

In conclusion it was found that the acoustic power delivered to the receptor vessel could be increased by the use of increased static pressure to limit the cavitation

(where it was not needed) and reduce the scattering of the sound beam, which produced positive results. The use of multiple transducers also produced good results when compared to the same vessel with only one transducer emitting sound. Unfortunately, the acoustic streaming was not evident in the multiple transducer vessel.

Through experimentation and confirmation with relevant theory, the factors affecting streaming and cavitation in this type of system were presented and an optimised system was achieved.

Table of Contents

		Page
Acknowledgments		**ii**
Declaration		**iii**
Synopsis		**iv**
1 Introduction		**1**
1.1	Previous Work	1
1.2	Scope and Limitations	2
1.3	Structure of the Thesis	3
2 Literature Review		**5**
2.1	An Overview of Ultrasonics	5
2.2	Cavitation	6
2.2.1	*Cavitation Threshold*	*6*
2.2.2	*Cavitation Strength*	*7*
2.3	Streaming	10
2.3.1	*Radiation Pressure*	*10*
2.3.2	*Acoustic Streaming*	*11*
Reflections & Transmission of Sound		12
2.3.3	*Reflection at Material Interfaces*	*12*
2.3.4	*Refraction at Material Interfaces*	*14*
2.3.5	*Absorption in Non-Cavitating Liquids*	*15*
2.4	Transducers	16
2.4.1	*Simple Harmonic Motion and Resonance*	*16*
2.4.2	*Equivalent Circuits*	*20*
2.4.3	*Types of Transducers*	*22*
2.4.4	*The Piezoelectric Effect*	*22*
2.4.5	*Transducer Construction*	*23*
2.4.6	*Transducer Efficiency*	*25*
2.4.7	*Amplitude Measurement Methods*	*26*

2.5 Thermal Considerations 27
2.5.1 Thermal Conduction, Heat Flow *27*
2.5.2 Convection in Liquids *28*
2.5.3 Heat Capacity *29*
2.5.4 Thermal equivalent circuits *30*

3 Experimental Method **31**

3.1 Experimental Set-up 31
3.2 Foil Method 33
3.3 Digital Image Processing 33
3.3.1 Analysis and Extraction of Damaged Areas *34*
3.3.2 Analysis and Extraction of Destroyed Areas *36*
3.3.3 Mean Deviation on Foil Samples *37*
3.4 Streaming 38
3.5 Temperature Measurements 39

4 Static Pressure **40**

4.1 Design of the Pressure Apparatus 40
4.1.1 Design and Experimental Conditions *41*
4.1.2 Plastic Bottle Sealing *44*
4.1.3 Comparison between Glass and New Pressure Vessel *44*
4.2 Pressure Effects on Transducer 46
4.2.1 Pressure Effect on Power *46*
4.2.2 Pressure Effect on Resonant Frequency *47*
4.3 Static Pressure Effect on Disruption 48
4.4 Differential Pressure Testing 50
4.4.1 Effects of Water Level Variations *50*
4.5 Conclusion 51

5 Tri-Reactor Vessel **52**

5.1 Experimental Apparatus 52
5.2 Design and Construction 53
5.2.1 Geometry *53*
5.2.2 Transducer Selection *54*
5.2.3 Resonance Modes *55*

5.3 Mapping the Sound Field 57
5.3.1 Focusing *57*
5.4 Optimising the Receptacle 58
5.4.1 Effects of Multiple Transducer on Receptacle Disruption *59*
5.4.2 Plastic Receptacles *60*
5.4.3 Receptacle material *61*
5.4.4 Streaming *63*
5.4.5 Triangular Vessel Receptacle *63*
5.5 Pressurizing 64
5.5.1 Pressure Effects on Resonant Frequency *64*
5.5.2 Pressure Effects on Power *65*
5.5.3 Differential Pressure Effects *66*
5.6 Comparison between Tri-reactor and Vibracel Unit 67
5.7 Conclusion 68

6 Transmission Media **69**

6.1 Acoustic Attenuation 69
6.1.1 Theoretical Transmission Calculations *70*
6.1.2 Attenuation in the System *71*
6.1.3 Affect of solutes on Vapour Pressure *73*
6.2 Transmission Media 74
6.2.1 Testing of Various Media *74*
6.2.2 Optimising $CaCl_2$ Solution Concentration *75*

7 Streaming **77**

7.1 Test Conditions 77
7.2 Acoustic Intensity 80
7.3 Distance from Transducer 81
7.4 Bottle Size 82
7.5 Volume Levels 83
7.6 Conclusion 83

8 Thermal Shocking **84**

8.1 Test Conditions 84
8.2 Effects of Temperature on Cavitation 86

8.3 Use of Analogue Computers in Temperature Calculations 87
8.4 Temperature Profiles 88
8.4.1 Varying Volume Ratios *88*
8.4.2 Equivalent Circuits *90*
8.4.3 Ultrasonic Energy Effects *91*
9 Conclusion & Future Recommendations **93**
10 References **95**
Appendix A **I**
Appendix B **II**
Appendix C **III**
Appendix D **IV**

1 Introduction

The object of this thesis was to investigate the factors contributing to and influencing ultrasonic dispersion, in an attempt to optimise both the cavitation and streaming effect associated with high power acoustics. This was done with the intention of designing and building an ultrasonic dispersion cell with a removable treatment vessel for the processing of a wide range of organic samples, thereby providing a stable, controllable platform for biochemical researchers.

In this context, dispersion is defined as a process where a solid is dissolved or at least broken down to small particles typically in a liquid medium. This has many industrial applications; high power ultrasound is being used to homogenise or mix paints, in breaking of micro-organism cells and as a catalyst to chemical reaction (due to the thorough micro-mixing properties of high intensity ultrasound).

1.1 Previous Work

This project was based on and a continuation of research by Ricardo de Quieros into ultrasonic dispersion. It is therefore important that the key issues of his findings are briefly discussed: [12]

A wide variety of ultrasonic apparatus and sources were experimented with, revealing the need for a high power (above 200 Watts) and high intensity system. The importance of delivering high intensity acoustic energy to the receptor vessel was obvious. A serious power saturation problem became evident during his research (where an increase in the acoustic power above 80 Watt would not increase the acoustic intensity in the receptor vessel). Mr De Quieros found that a commercial unit, the VCX500 manufactured by Vibracel, provided a flexible powerful (up to 500

Watts) system in which to conduct optimisation experiments and, as a result, that became the main ultrasonic source used in this project. [12]

There is much work on the effect of high power ultrasound and the many areas that have been advance by using ultrasonic properties. C. Suri (et al) present a system that has similarities to this project in that the streaming properties are used to mix liquids in a chemical reaction vessel, therefore acting as a catalyst. The streaming is generated with the use of two transducers in different planes and measured with the aid of an iodide solution, a laser and a receiver diode arrangement. This system, however, only uses the streaming effects of high frequency ultrasound and therefore does not consider cavitation. [13]

N.A. Tsochatzidis (et al) describe a method of cavitation cloud measurement where a laser is passed through the cavitation cloud, using Doppler shift to give velocity and cavitation bubble average size. [14] Yet another advanced method of cavitation cloud measurement makes use of X-ray equipment to take snap shots of cavitation fields. [15] Although these methods of measurement are complex and costly, they show the cutting edge in ultrasonic effect measurement.

1.2 Scope and Limitations

This project was primarily concerned with the investigation into the effects of cavitation and streaming in terms of their ability to disperse or process a wide variety of biological samples for research purposes. The intention of the project was not to investigate the effects of ultrasound on biological samples but to provide a stable, well-defined platform so that experts in their respective fields can conduct research using high power ultrasound. In order to achieve this, both the cavitation and the streaming effects need to be consistently reproduced and the factors influencing them need to be well understood within the context of the project. The requirement that the treatment vessel should be removable is what sets this project apart from a typical ultrasonic cleaning bath, and significantly complicates the design. A major limitation on this design is the FDA's (Food and Drug Administration's) rules and regulations on

permissible materials and other possible contaminating effects on the organic samples, as it is envisaged that this device will be used, among other things, in the food industry. In the original design requirements the removable processing vessel was to be of a small volume, less than one hundred millilitres.

1.3 Structure of the Thesis

Introduction: An explanation of the project's main research objectives, restrictions and scope, as well as a short review of previous, (including the most recent) work in the field.

Literature review: This chapter contains a comprehensive review of previously done work relating to this project, including both theory and practical tests done with specific application to this project.

Experimental Methods: This chapter contains information on the basic experimental set-up that explains methods of quantifying both streaming and cavitation fields. It also considers the mean error or accuracy involved in these methods.

Static Pressure: This chapter looks at the construction/adaptation of an ultrasonic vessel to study the effects of static pressure on cavitation threshold and its disruptive ability. Included is a discussion on the effects of static pressure on the transducer and electronics.

Tri-reactor Vessel: This chapter looks at the design and testing of a three-transducer bath with the intention of gauging the effectiveness of using multiple transducers in a dispersion system. The combination of static pressure and the multiple transducers is also investigated.

Transmission Media: This chapter considers a wide variety of materials for their acoustic transmission of high power ultrasound. This was primarily aimed at

cavitation suppression but also attempted to match acoustic impedances as best as possible for real liquids.

Streaming: This chapter investigates the factors affecting acoustic streaming in the receptor vessel, in terms of its velocity and magnitude and the factors which affect them.

Thermal Shocking: This chapter looks at the uses of rapid temperature cycling to assist in the dispersion process. A method of estimating real temperature profiles based on measured temperatures is presented.

Conclusion and Future Recommendations: A review of relevant findings and how they affect the design of an ultrasonic dispersion unit as a whole, as well as other possible areas for further research.

2 Literature Review

This chapter consists of a review of the work done by others in the field of ultrasound and other relevant areas. It begins with a brief overview and background into ultrasound and then goes on to discuss the fundamental effects of high power ultrasonics, with the core focus being on cavitation and streaming. It is then followed by an investigation into reflection and transmission of sound at material boundaries and through materials respectively. Transducer's modes of operation and various related physical properties are discussed, since transducers form an integral part of any ultrasound research. Lastly, a thermal theory was presented, as temperature plays an important role in a solvent's ability to dissolve, as well as affecting cavitation.

2.1 An Overview of Ultrasonics

Ultrasound, very simply, is a sound wave whose frequency is too high for the human auditory system to hear – typically from 18 kHz upwards into the MHz range and beyond. Over the past few years ultrasound has been used in many new applications including imaging (medical as well as mechanical spheres), water purification, distance measuring devices, food processing and many other areas that are still being developed. [3] [16]

2.2 Cavitation

As already mentioned, cavitation and streaming perform an integral role in sonic processing. Cavitation provides a disruptive force required to breakdown samples, while the streaming provides the macro mixing quality. Together they create an effective homogenisation mechanism. Both cavitation and streaming occur at similar acoustic intensities, but other than that they are distinctly different in terms of the factors that influence their magnitudes and occurrence. This section considers the factors causing cavitation and the physical properties contributing to its strength. It then goes on to discuss radiation pressure and the factors influencing acoustic streaming. [2] [1]

2.2.1 Cavitation Threshold

Cavitation, loosely defined, is a rupture or cavity that is formed in a liquid when the tensile force on the liquid molecules is larger than the vapour pressure. These cavities subsequently collapse violently, sending out shock waves and causing powerful micro jetting sufficiently destructive to erode metal surfaces. Micro jetting defines a situation when a bubble collapses from one side sending a small jet of high velocity liquid through the bubble and out the other side. [20]

The pressure required to initiate cavitation would have to be of the order of 1000 atm for water in theoretical calculations. However, the presence of minute gas bubbles and impurities in real liquids provide a non-uniformity around which a cavity can form at much lower tensile forces. These gas bubbles or impurities are called cavitation nuclei and are the source of most common cavitations. The tensile force in the ultrasonic context is provided by an oscillating sound field, which creates a sinusoidal by varying pressure. During the rarefaction stage, a saturated vapour filled bubble forms in the liquid. This bubble then, (during the compression stage) collapses due to the high pressure aided by surface tension pulling the bubble closed. The pressure threshold that cavitation occurs at is governed by the equation below. [4]

$$P_{thres} = P_{sat\_vap} + P_{static} + P_{gas} - 2\sigma/R_0$$ **Equation 2-1**

Where σ is surface tension and R_0 is initial bubble radius. This shows that an increase in vapour pressure (P_{sat_vap}) or static pressure (P_{static}) increases the threshold pressure (P_{thres}). The increasing of threshold pressure has the effect of suppressing cavitation. However, if one increases the sound pressure above the threshold pressure, the liquid will again begin to cavitate. The simultaneous increasing of both the sound and threshold pressure would not cause an increase in cavitation strength, as one would expect. The factors influencing cavitation strength will be discussed in the next section. [4]

The equation:

$$P_{thres} = 0.7(T_{boil} - T) + 1 \quad [\text{Atm}]$$ **Equation 2-2**

gives an estimate of threshold pressure as a function of liquid temperature. It is interesting to note that the boiling point (T_{boil}) is used in the calculation, implying that if one increases the boiling point of a liquid it will raise the threshold pressure. This correlates with the above reference to saturated vapour pressure because boiling point is linked to vapour pressure. Thus it can be seen how temperature, vapour pressure and static or atmospheric pressure affect the cavitation threshold. [2]

2.2.2 Cavitation Strength

The strength of cavitation, among other things, is proportional to the ratio of maximum bubble radius over initial bubble radius $\frac{R_{max}}{R_0}$ [2]. This makes sense when looking at where the energy that is released during a cavitation comes from. It originates primarily from surrounding liquid rushing into the cavity. The larger the cavity radius just before collapse and the less gas in the initial bubble, the larger the

compressive forces on the bubble, leading to a rapid and violent collapse. If one wants to decrease the initial bubble size the cavitation nuclei size needs to be reduced. This can be achieved by degassing and removing all impurities from the liquid. The effect is that the cavitation becomes more vaporous in nature, and is known for being more violent. This is because there is very little gas in the bubble to hold it open, as the vapour under the high pressures dissolves back into the water when the cavity collapses. [2] The violence of the cavitation can be increased by increasing the sound pressure. However, this will only work up to the point where the liquid starts cavitating in another region (i.e. between the intended region and the transducer) as this causes the sound beam to be scattered and absorbed by the misplaced cavitation before it gets to the area intended for treatment. Hueter and Bolt [2] describe a method of overcoming this saturation problem, which involves having a pressurised transmission medium and a sound transparent window allowing the sound beam to pass into the target area.

Another factor that increases the strength of cavitation is the surface tension (σ) where $2\sigma/R_0$ represents the inward pressure on the bubble exerted by the surface tension pulling it closed. If the surface tension is increased, it will once again increase the forces involved during collapse and lead to more violent cavitation. However, an increase in surface tension will also require an increase in sound pressure to form, and grow, the cavity bubble. [2]

The temperature of the cavitating liquid (in this case water), according to Hueter & Bolt, affects the cavitation strength. Graph 2-1 shows relative weight loss on brass as a function of temperature for a 575 KHz system. This may be because the change in temperature is changing the cavitation threshold, limiting the number of cavitation bubbles and so reducing the damaging effect. Hueter & Bolt also go on to say that vapour pressure, and hence temperature, affects the maximum size of the bubble, thus altering the strength of the cavitation [2].

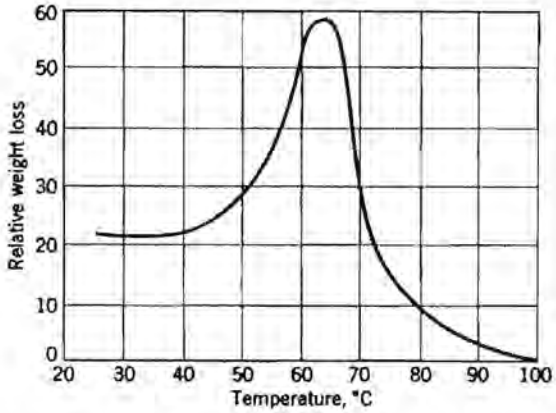

Graph 2-1 Relative Weight Loss in Cavitation Erosion as a Function of Temperature [2] Pg 235

M. H. Entezari (et al), using the oxidation of iodine to measure cavitation intensity in a 20 KHz system, found the cavitation strength to falloff with an increase of temperature, and attributed this to more vaporous type cavitation occurring at lower temperatures. M. H. Entezari (et al) also present a graph of similar shape to that in Graph 2-1 for a 900KHz system, showing the effect of different frequencies on cavitation strength where temperature is concerned. Based on these findings a lower temperature would be better for violent cavitation at 20Khz. [19]

M. H. Entezari (et al) conducted tests varying the gas content of the liquid, using the same iodine oxidation rate as an indicator, concluding that the effect of introducing gas had little effect at 20 kHz [19]. This finding is contrasted by other researchers' findings that state that the introduction of gas bubbles reduces the vaporous type cavitation. [2]

2.3 Streaming

As already mentioned, acoustic streaming is responsible for mixing and stirring in the treatment vessel. Obviously, the more pronounced the streaming effect, the better, as this will cause a more thorough mixing and stirring action.

2.3.1 Radiation Pressure

There are many possible causes of radiation pressure and, subsequently, streaming, but in this environment it is most likely a combination of Radiation and Oseen forces. Radiation forces are primarily due to the scattering of sound waves on impurities and, of course, cavitation bubbles. Oseen forces are generated by ultrasonic wave distortion, which is due to non-linearities in the liquid (caused by cavitation, among other things). The drag coefficients of the two forces, which give a measure of the radiating force, are as follows: [2]

Radiation Forces $1.2(kr)^4$ **Equation 2-3**

Oseen Forces $\frac{3}{\pi} c_2 \sin\varphi$ **Equation 2-4**

where k is ω/c (Frequency over sound velocity), r is the particle radius, $c_2 = u_2/u_0$ is the fractional second harmonic content (amount of the wave which has distorted to its second harmonic) and φ is the phase shift between the fundamental and the second harmonic.

2.3.2 Acoustic Streaming

Acoustic streaming is simply the reaction of a fluid to the forces discussed above. The fluid motion is also affected by factors such as viscosity, density and physical restraints of the vessel. As a result, the streaming theory becomes a complex problem that is case specific. The equations in the section entitled Radiation Pressure give an idea of the factors influencing streaming. In Shutilov [4] and Beyer [8] it is stated that the streaming is proportional to the total acoustic absorption coefficient of the fluid. This correlates with Oseen forces, as the harmonic distortion is a form of absorption in the liquid.

Shutilov [4] gives the following equation for calculating this absorption coefficient:

$$\alpha_0 = \frac{2}{3}\frac{\omega^2 \eta_s}{\rho_0 c_0^3} \quad [4] \text{ pg } 145 \qquad \textbf{Equation 2-5}$$

The velocity of the streaming in an unbounded situation is given by:

$$v_0 = \frac{I_0 R^2 \omega^2}{3\rho_0 c_0^4} \quad [4] \qquad \textbf{Equation 2-6}$$

Dymling (et al) gives a simplified equation for streaming velocity

$$v_0 = \frac{\alpha P Y}{\mu c_0} \quad [18] \qquad \textbf{Equation 2-7}$$

where both μ and η_s are the coefficient of viscosity, I_0 is acoustic intensity, R is particle radius, ρ_0 is the mean density, c_0 is the mean sound speed, P the average acoustic power, Y a geometry coefficient, and α is the absorption coefficient

The amount and velocity of streaming is proportional to ω^2. This is unfortunate because cavitation is more pronounced at low frequencies; however if one needs more acoustic streaming and can afford to reduce the cavitation this could be done by increasing the frequency of the sound wave. [19] It is must also be noted that increased viscosity increases the absorption, and therefore the streaming magnitude, but decreases the streaming velocity according to Equation 2-7, and that streaming velocity is proportional to acoustic intensity. [4] [18]

Reflections & Transmission of Sound

The transmission of sound is of great importance in terms of the delivery of maximum acoustic intensity, as well as the use of reflection boundaries as a mechanism for creating standing waves. This section begins with a discussion of sound wave reflection at material interfaces or boundaries and then goes on to look at some of the factors influencing the absorption in liquids that are not cavitating.

2.3.3 Reflection at Material Interfaces

The explanation of reflection and transmission, for the time being, will be restricted to orthogonal incident waves, but will be extended to other angles of incidence. As is well known, sound waves, such as a loud shout, are reflected off cliff faces, echoing back. The precise amount of sound energy that is reflected by and transmitted through a medium interface can be calculated using the two media's acoustic impedances.

The accoustic impedance (Z) is calculated from two physical properties, namely the product of density (ρ) and sound speed (c). This is very useful if one wants to manipulate the amount of reflection/transmission at medium interfaces. There are four variables that can be tuned: density and sound speed for both of the media.

$$Z = \rho c \qquad \textbf{Equation 2-8}$$

Figure 2-1 shows an incident wave represented by A_i, the reflected wave A_r and the transmitted wave B_t.

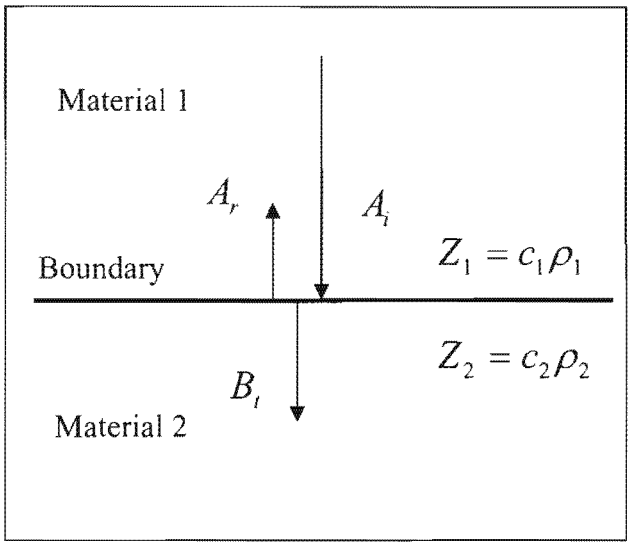

Figure 2-1 Sound Wave Reflection and Transmission [8] Pg 48

The amount of energy reflected is calculated by

$$A_r = \frac{Z_1 - Z_2}{Z_1 + Z_2} A_i \quad \text{[8] Pg 49} \qquad \textbf{Equation 2-9}$$

and the amount of energy transmitted is calculated by

$$B_t = \frac{2Z_1}{Z_1 + Z_2} A_i \quad \text{[8] Pg 49} \qquad \textbf{Equation 2-10}$$

Although the above discussion is limited to orthogonal wave material boundaries, the two above equations may still be used for magnitude calculations for the orthognal components in the next section and the angles are calculated as shown in the following sub-section.

2.3.4 *Refraction at Material Interfaces*

As mentioned previously, the magnitudes of the reflected and transmitted rays can be calculated by the above equations for all angles of incidences. Figure 2-2 shows an incident sound wave at an arbitrary angle θ_i, measured from the normal. The angle of the reflected ray is such that $\theta_i = \theta_r$.

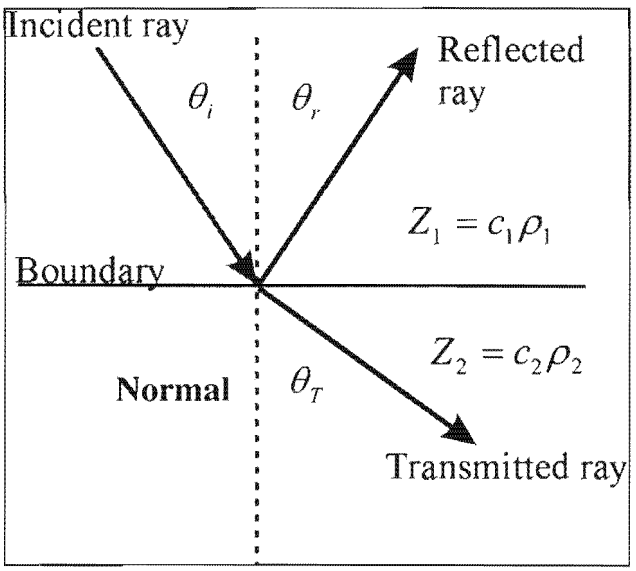

Figure 2-2 Sound Wave Refraction

The angle of the transmitted wave is calculated by the following equation

$$\frac{\sin\theta_i}{c_1} = \frac{\sin\theta_T}{c_2}$$

Equation 2-11

where the angle of refraction can be altered by changing the speed of sound of the material. This provides flexibility in terms of making acoustic lenses that transmit most of the sound energy (i.e. similar Z), yet can be tuned to have suitable refractive indices (by varying ρ inversely to c). [8]

2.3.5 Absorption in Non-Cavitating Liquids

The absorption of sound in a non-cavitating liquid is primarily caused by the frictional or viscous damping and, consequently, heating.

$$I_x = I_0 e^{-2\alpha x}$$ **Equation 2-12**

gives the intensity of the sound as a function of distance x, which is an exponential falloff where the absorption coefficient, α, is determined by the sum of the internal friction of the liquid and the conduction as shown below:

$$\alpha = \alpha_r + \alpha_l$$ **Equation 2-13**

Where Internal friction according to Stokes is

$$\alpha_r = \frac{8}{3}\frac{\pi^2 \varpi^2 \eta}{c^3 \rho}$$ [3] Pg 128 **Equation 2-14**

and Conduction (Kirchoff)

$$\alpha_l = \frac{2\pi^2 cKTa^2}{\Lambda^2 \rho W C_p}$$. [3] Pg 129 **Equation 2-15**

In the above equations ω is sound frequency, η is viscosity, c is sound velocity, ρ is the density, K is the thermal conductivity, T the temperature in Kelvin, a the thermal coefficient of expansion, Λ the wavelength, W the mechanical equivalent of heat and C_p the specific heat of the liquid. A large α would result in a rapid falloff in sound intensity as waves travel through a liquid. To reduce the absorption in the liquid the sound frequency and the viscosity should be reduced, and the sound speed and density should be increased, among other things.

2.4 Transducers

Transducers are responsible for the generation of ultrasonic energy or, more precisely, the conversion of energy from one form to another (in this case electrical to mechanical energy). Modern transducers make use of a complex combination of electrical and mechanical properties of various materials to create an ultrasonic source. It is therefore important that this section explains the principles of simple harmonic motion and resonance, the implications for transducers, and the use of equivalent circuits for a simple analysis of transducers. In addition to this, various types of transducers are discussed, the operation of piezoelectric materials is then explained and, finally, a few critical properties of transducers are mentioned.

2.4.1 Simple Harmonic Motion and Resonance

In order to explain simple harmonic motion and to create an intuitive understanding of how a system would resonate, a basic example of a mass on the end of a spring will be used to lay a foundation.

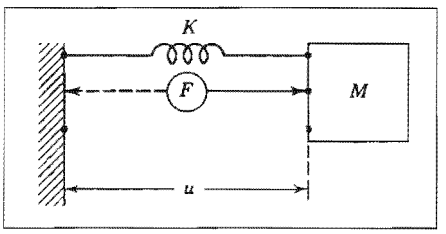

Figure 2-3 Mass and Spring [2] Pg 14

In the system shown in Figure 2-3 above, there are two potential forces being exerted on the mass: firstly, the force exerted by the spring which is proportional to the displacement, but in the opposite direction to the displacement as defined by the equation $F_s = -Ku$, where K is Hooke's spring constant as defined by Hooke's law and u is displacement; secondly, the force as a result of acceleration that is in the same direction as the acceleration as defined by the equation $F = ma$ where m is the

mass. When we sum forces and set the sum equal to zero, a differential equation is obtained:

$$m\frac{d^2u}{dt^2} + Ku = 0$$ **Equation 2-16**

Using the particular solution: $u = U\cos(\omega t)$ we get:

$$\frac{d^2u}{dt^2} = -U\omega^2\cos(\omega t) = a$$ **Equation 2-17**

Substituting into Equation 2-16 we get:

$$mU\omega^2\cos(\omega t) + KU\cos(\omega t) = 0$$ **Equation 2-18**

Solving this produces the above equation describing the displacement of the mass that is shown in Graph 2-2 below (assuming initial conditions are correct). From this equation we can calculate the frequency at which the displacement of the mass will oscillate, giving its resonant frequency (the frequency at which it will oscillate if disturbed once and then left to oscillate).

$$\omega_0 = \sqrt{K/m}$$ **Equation 2-19**

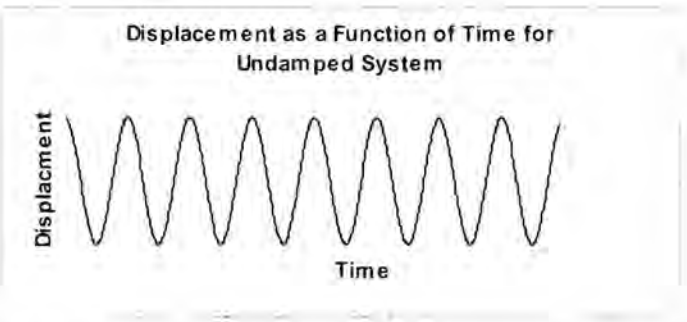

Graph 2-2 Displacement vs Time Undamped Oscillations

It is relevant to note that if the stiffness is increased and/or the mass is reduced, the resonant frequency increases. The converse is also true if the frequency needs to be decreased: the stiffness should be reduced and /or the mass increased.

However, this is not a very realistic solution, as it does not include any velocity related forces such as friction or damping. This frictional force, which is proportional to but in the opposite direction of the velocity, is then introduced into the differential equation giving:

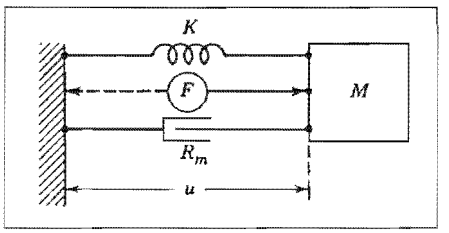

Figure 2-4 Mass, Damper and Spring [2] Pg 14

$$m\frac{d^2u}{dt^2} + R_m\frac{du}{dt} + Ku = 0 \qquad \textbf{Equation 2-20}$$

Which can be solved to give

$$u = U\cos(\omega t)e^{-\kappa t} \qquad \textbf{Equation 2-21}$$

It is once again solved to reveal the characteristic equation, which is a sinusoid falling off exponentially as shown in Graph 2-3 below, where

$$\kappa = \frac{R_m}{2m} \qquad \textbf{Equation 2-22}$$

and the resonant frequency is

$$\omega_f = \sqrt{\omega_0^{\,2} - \kappa^2} \qquad \textbf{Equation 2-23}$$

or more fully

$$\omega_f = \sqrt{\frac{K}{m} - \left(\frac{R_m}{2m}\right)^2} \qquad \textbf{Equation 2-24}$$

This implies a decrease in resonant frequency when the frictional force is increased. Again, increasing the mass will decrease the frequency as the $\frac{1}{m}$ term will dominate over the $\left(\frac{1}{2m}\right)^2$ term.

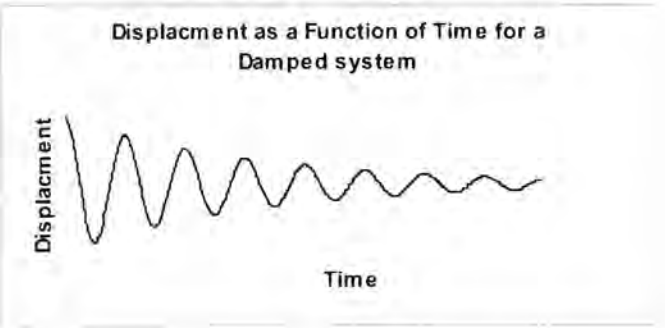

Graph 2-3 Displacement as a Function of Time for a Damped System

If we look at the frequency response in Graph 2-4 for an arbitrary system the effect of stiffness, mass and damping become clear.

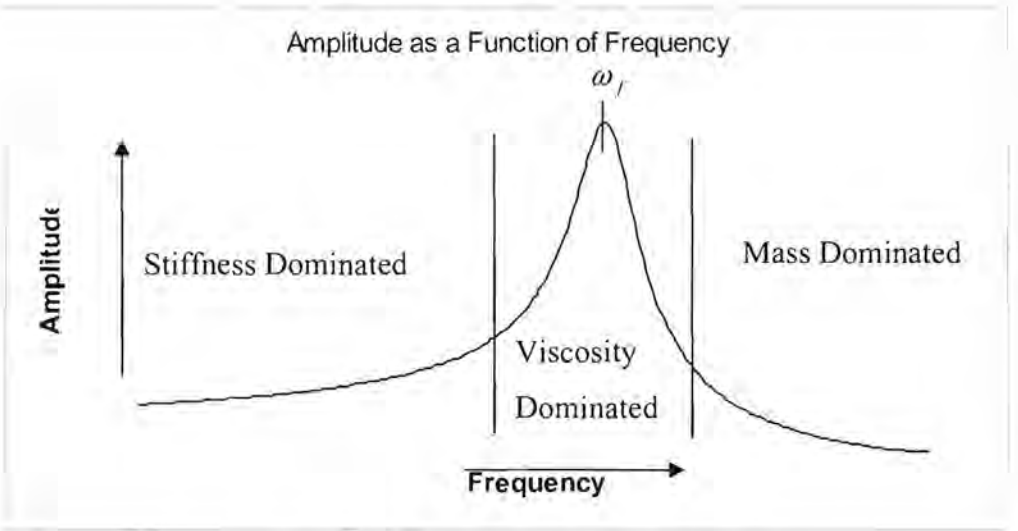

Graph 2-4 Frequency Response [2] Pg 18

We now have a more realistic model for explaining resonance in solids as most material characteristics can be approximated by viewing them as a set of springs, masses and damping forces. However, this is not entirely accurate as factors such as Passion's ratio and non-linearities in the materials' stress/strain curves have not been taken into account. Including these factors in the analysis would prove to be very time-consuming and this added computation would not necessarily assist in a practical understanding of this project. As a result the fore-mentioned factors will not be dealt with in detail.

2.4.2 Equivalent Circuits

Transducers are generally driven by an electrical source that sees the transducer as an electrical load. For this reason it is useful to be able to express the mechanical parameters and properties of the transducer in terms of its electrical equivalent. This can also serve to extend one's understanding of the mechanical system if one looks at the equivalent electrical circuit [5] Pg 73.

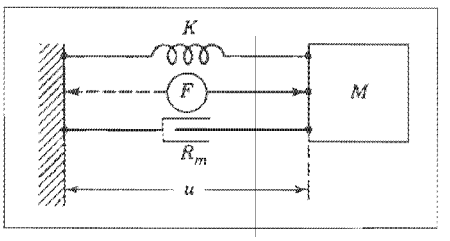

Figure 2-5 Mechanical System [2] Pg 14

$$m\frac{du}{dt} + ru + K\int u dt = F_0 e^{j\omega t}$$ **Equation 2-25**

The characteristic differential equation that describes the above example of a resonating mechanical system shown again here in Figure 2-5 can also be expressed as an equivalent electrical circuit of an inductor, capacitor and resistor in series as shown in Figure 2-6. Table 2-1 gives a list of mechanical parameters and their equivalent electrical parameters. (Note that a parallel mechanical system is expressed as a series electrical system and vice versa.)

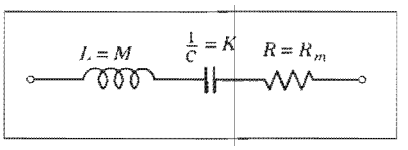

Figure 2-6 Electrical System [2] Pg 14

$$L\frac{di}{dt} + Ri + \frac{1}{C}\int i dt = V_0 e^{j\omega t}$$ **Equation 2-26**

Mechanical	Electrical
Mass	Inductance
Compliance*	Capacitance
Resistance	Resistance
Velocity	Current
Force	Voltages
Displacement	Charge
Impedance	Impedance

Table 2-1 Equivalent Parameters [5] Pg 75

This use of equivalent circuits enables the use of powerful electrically based circuit theory to solve and explain the mechanical system. Similarly, the electrical power being delivered to the transducer and other factors can be used to calculate acoustic power from electro-mechanical efficiency that is again electrically calculated from the impedance.

* Compliance is the reciprocal of stiffness.

2.4.3 Types of Transducers

Ultrasonic waves are primarily generated with electro-mechanical transducers such as those using piezoelectric crystals that are discussed in the section below. However, there are other ultrasound generators, namely whistles and sirens, which use entirely mechanical means to create tensile forces high enough to cause cavitation. These are generally used in high volume industrial processes. Another common electro-mechanical method of creating ultrasound is with the use of a magneto-strictive transducer that makes use of the electromagnetic properties of certain metals to create a mechanical vibration. These were very common in the 1950's, but they have now been superseded in most areas by piezoelectric technology and will not be investigated further in this thesis. [5]

2.4.4 The Piezoelectric Effect

Piezoelectric transducers have found wide acceptance because of their ability to convert electrical energy to mechanical energy at high efficiencies as well as being able to reverse the process i.e. to convert mechanical energy into electrical energy also at high efficiencies. [5] Piezoelectric transducers have been in common use for over forty years and as a result there are many commercial transducers on the market.

2.4.4.1 How Piezoelectric Materials Function

The internal mechanisms that give piezoelectric materials their properties are illustrated in Figure 2-7, where the crystalline structure is shown. When a stress is applied to the crystal a change in dimensions, known as strain, results. This has the effect of squashing the lattice so that more positive molecules (in this case) are at the bottom and the majority of the negative molecules are at the top, creating a potential difference between the two surfaces of the crystal. The converse of this process is also true: if a voltage is placed on the crystal surfaces, it pulls the molecules to compress the crystal resulting in a strain, which in turn would cause a stress if the crystals were fixed to rigid supports.

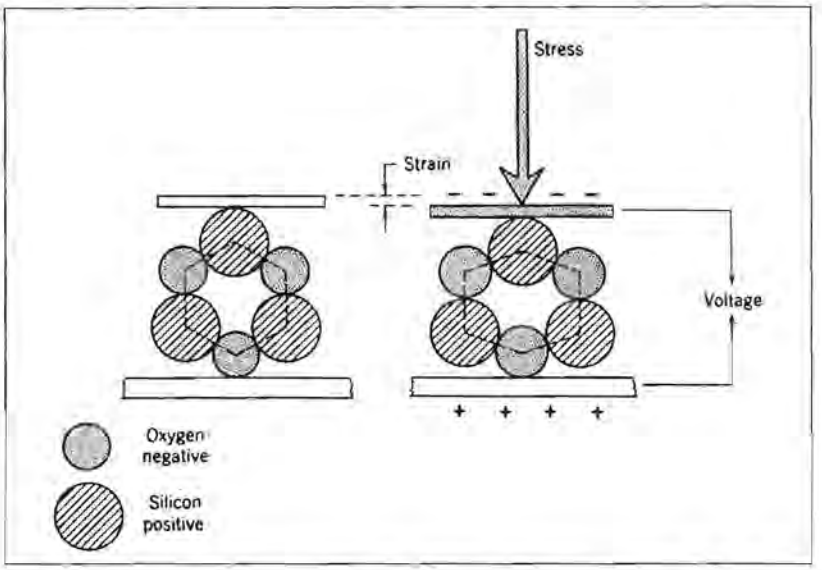

Figure 2-7 Piezoelectric Crystal's Internal Structure [2] Pg 88

These crystals are typically made of ceramics such as Barium Titanate and Lead Zirconate Titantate (PZT) that are cast in a large electric field, orientating the charged molecules in the ceramic before it sets.

2.4.5 Transducer Construction

The design and construction of transducers is as varied as the possible applications, from trial and error methods, to modern Finite Element numerical methods, using large amounts of computing power. This discussion will focus on one particular transducer design that was used in this project.

The most important component of any transducer is its active component: in this case, the two PZT discs. Two separate discs are used, among other things, to ensure that both the front and back masses stay at the same potential to avoid harmful electrical shocks, as the voltages involved can be as high as 1 kV_{p-p}. The process of making the PZT ceramic as explained yields an efficient and linear piezoelectric material. These are unfortunatly brittle, in particular having little strength in tension. For this reason it is necessary to bias the PZT with a constant compressive force to ensure that it is never operating in tension. This is normally achieved with the use of a centre bolt that

clamps the crystals and provides a fixing point for the front and back mass. (See the exploded assembly in Figure 2-8.)

The front and back masses are designed to assist the PZT to resonate at the correct frequency and, in the case of the front mass, to provide an emitting surface that can support the high stresses in both compression and tension that are involved at high powers. This transducer is face-mounted on a thin steel plate and it is, therefore, not necessary to have nodal point (point of little or no movement on the transducer) mountings, which simplifies the design greatly.

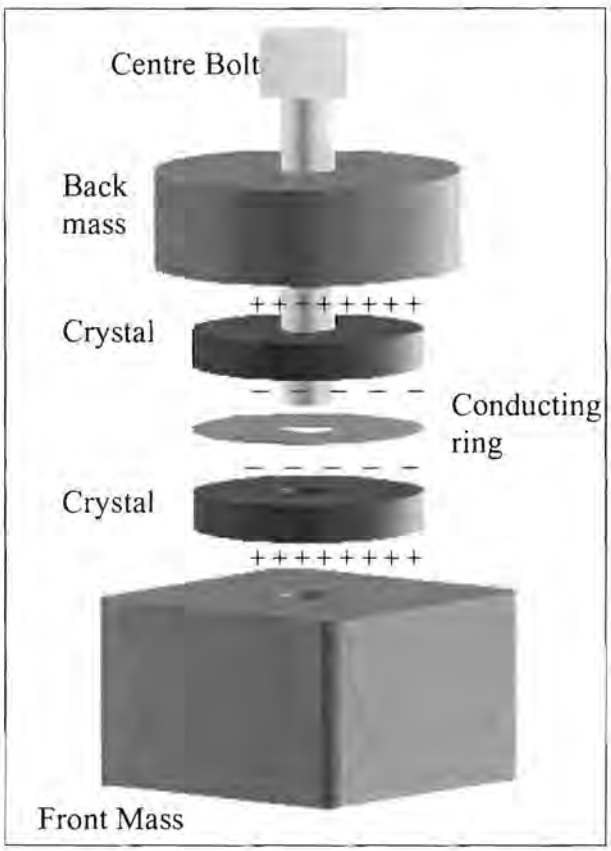

Figure 2-8 Transducer Assembly

2.4.6 Transducer Efficiency

If one looks at an equivalent circuit for a typical transducer as in Figure 2-9, the LCR series circuit can be seen. This is named the 'motional arm' because it represents the mechanical part of the transducer. The power dissipated in the 'motional arm' is the same as mechanical power of the transducer. If one applied a mechanical load to the transducer it can be seen as an electrical load in the 'motional arm', which would result in an increase in resistance of the 'motional arm'. This increase in resistance can be used as a coupling factor (to the load) and so give the efficiency of the transducer. Equation 2-29 calculates this increase as a ratio giving efficiency (assuming R_i does not change significantly in water). [5]

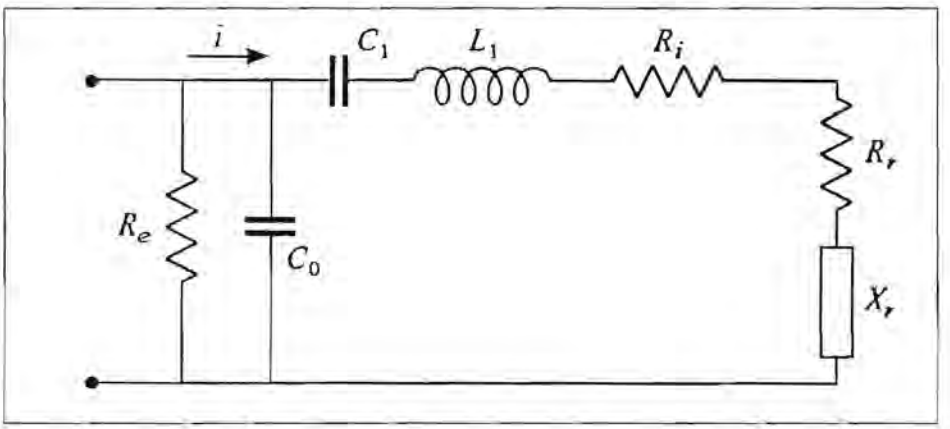

Figure 2-9 Transducer Equivalent circuit showing Internal Losses [5] Pg 86

R_i represents internal mechanical losses, R_r the radiation resistance and X_r is the radiation reactance of the water (load). R_e and C_o are the clamped admittance where the losses are directly proportional to the applied voltage. [5]

$$G_{load} = \frac{1}{R_i + R_r}$$ **Equation 2-27**

$$G_{air} = \frac{1}{R_i}$$ **Equation 2-28**

Mechanical – acoustic efficiency

$$\eta_{ma} = \frac{R_r}{R_i + R_r} = \frac{G_{air} - G_{load}}{G_{air}}$$ **Equation 2-29**

2.4.7 Amplitude Measurement Methods

If consistent, reproducible ultrasonic intensities are required, it is important to maintain constant amplitude at the emitting surface of a transducer. It is therefore necessary to measure this amplitude. This can be achieved very accurately with a microscope, but this method of measurement does not lend itself to a practical/real-time measurement or to feedback control systems. It is for this reason that designers use current feedback in transducers' amplifiers. In the equivalent circuit section, it can be seen that the current's equivalent parameter in mechanical terms is velocity. Using velocity for amplitude measurement seems incorrect, however if one integrates the current it will give transducer displacement. As a result the current can be used as a relatively good approximation of amplitude. If a device is said to be using current feedback it implies that it controls the power being transmitted to the transducer by looking at the current. This is the mechanism that the Vibracel ultrasonic source uses to control the amount of power being delivered to the transducer to maintain a set amplitude.

2.5 Thermal Considerations

In a project of this nature where the temperature is critical in terms of its effect on cavitation threshold, the ability of a solvent to dissolve, and to some extent to the operation of transducers, it is important to understand the modes in which temperature is reduced, maintained and transmitted. In this project we have a situation where the ultrasonic transducers are putting energy into a system in which most energy results in heating. It is important to understand the difference between heating energy and temperature. Heating energy is the mechanism or source that causes a rise in temperature i.e. the flow of thermal energy out of a system will cause a decrease in temperature. There are three modes in which temperature can be transmitted: convection, conduction and radiation. Convection and conduction will be discussed below, as these are the two main modes of heat transfer that will be encountered in this project. Another important property of materials that will be discussed is heat capacity or a measure of the "energy required to raise the temperature of a unit mass of a substance by one degree" [6].

2.5.1 Thermal Conduction, Heat Flow

Thermal conduction is the process whereby heat energy flows from one material to another, always from a higher temperature to a lower temperature. This is usually through some form of transmitting medium. The thermal conductivity of a material is an indication of its ability to transmit heat energy and so reduce the temperature of the hot material.

$$\dot{Q}_{cond} = k_t A \frac{\Delta T}{\Delta x}$$ **Equation 2-30**

Where $\dot{Q}$ is heat energy transfer rate, k_t is the thermal conductivity coefficient, A the area through which the energy is passing, Δx the thickness of the material and ΔT the temperature difference.

In looking at the equation for heat transfer through an object, it can be seen that an object of high thermal conductivity, large transmitting surface area, low thickness and high temperature gradient or temperature difference produces a large heat flow. To give an indication of the conductivity of certain relevant materials the table below is provided. [6].

Material	Thermal Conductivity W/m.k
Aluminium	237
Titanium	46.73
Glass	1.4
Poly Propylene	0.15
Water	0.613
Air	0.026

Table 2-2 Table of Thermal Conductivity [6] Pg 107

2.5.2 Convection in Liquids

Convection is similar to conduction in that it transfers its heat energy to a fluid using conduction, and then the fluid moves to a cold surface and heat energy from the fluid is transferred for a second time through conduction to the cold surface. There have been equations derived to calculate the heat transfer through convection. However, these are less exact than the equations for conduction. The reason for this is that the convection coefficient can vary from 50 to 1000 for free convection of liquids depending on many geometrical factors. This gives a huge variation in heat transfer, but still, the general underlying effects and principles can be extracted from equations for convection heat flow below.

$$\dot{Q}_{conv} = hA(T_s - T_f)$$ **Equation 2-31**

Where $\dot{Q}$ is heat energy transfer rate, h is the thermal convection coefficient, A the exposed area , T_f and T_s the temperature of the fluid and solid respectively.

From the equation it can be seen that the higher the convection coefficient, the larger the area, and the larger the temperature difference between the solid and the fluid, the higher the heat transfer through convection will be. Although very little can be ascertained from the coefficient, there is a clear advantage of introducing forced convection as the coefficient can go as high as 20,000. This is not an immediately obvious effect of acoustic streaming but an extremely important one nonetheless, as the acoustic streaming provides forced convection.

2.5.3 Heat Capacity

As already mentioned the heat capacity is a measure of a material's ability to absorb energy for a certain increase in temperature. This mechanism will not be discussed in detail but this effect needs to be kept in mind when using temperature increase as a measure of acoustic power. This is particularly relevant between two different devices as they may be made of different materials with different heat capacity, causing a large error in the results.

Material	Specific Heat (J/(kg.K))
Aluminium	910
Titanium	532
Glass	837
Poly Propylene	1800
Water	4190
Air	0.026

Table 2-3 Table of Specific Heat [6] Pg 107

2.5.4 *Thermal equivalent circuits*

Once again equivalent circuits can be used to solve thermal systems using electrical analysis techniques and analogue computers. The thermal and electrical systems are more similar than the mechanical and electrical systems, in that a parallel thermal system has an electrical circuit where the equivalent components are also in parallel. Table 2-4 gives the thermal and electrical equivalent physical parameters.

Thermal	Electrical
Temperature	Voltage
Heat flow ($\dot{Q}$)	Current
Mass . heat capacity	Capacitance
Conductivity . Area	Resistance

Table 2-4 Equivalent Thermal Parameters

3 Experimental Method

This chapter considers equipment and methods used in measurement and presentation of the results. Firstly, it looks at the typical set-up of equipment used in this project (transducers, temperatures, solvents etc.) based on previous work done by Mr De Quieros.[12] It then discusses the use of foil samples placed in the cavitation field and the image processing software used to analyse the damaged samples. Next it looks at the accuracy and reliability of the foil-image processor method as a whole. The method used to capture and analyse streaming in receptor vessels is then briefly reviewed. Finally the measurement of temperature in the thermal profiles is addressed, as well as the use of equivalent circuits to accurately estimate the real temperatures.

3.1 Experimental Set-up

This section will consider the physical parameters of a typical or base set-up for most experiments in this project. The relevant chapters then explain the slight variation of particular parameters.

As this was a continuation of research, a brief review of the previous equipment and method used by Mr De Quieros is appropriate. A wide variety of ultrasonic baths with

frequencies from 20 – 30kHz, horns, and cup horns (20 kHz) were experimented with, using a number of different receptor vessels of differing size, shape and material in various orientations. Based on the conclusion and recommendations of Mr De Quieros, a good set-up had been achieved, but needed further optimisation. This recommended set-up, which was used as a basis for this project, consisting of a titanium 64mm diameter cup horn manufactured by Vibracel with a 500 Watt amplifier – transducer combination. The cup that contained the transmission fluid was made of glass and fixed to the horn by a plastic screw-in lug. The receptor vessel was placed vertically in the cup horn with the base as close as possible to the emitting surface of the transducer (typically with a 1mm gap). The receptor vessel recommended was a 50ml polypropylene pill bottle. Various solvent and transmission media levels (height above the emitting-face) were experimented with, resulting in the finding that a level of 30-35mm was optimum for disruption. As temperature plays an important role where cavitation and chemical reactions are concerned, it was decided to use a cooling arrangement where the transmission medium would also serve the function of cooling. The temperature in the receptacle started at 23°C and was held below 39°C (this was part of the design requirements) by circulating the cooling fluid and limiting the sonification time. This cooling method unfortunately introduced a number of minute bubbles or cavitation nuclei that can alter the cavitation threshold slightly. In this project, this problem was solved by ensuring that the flow rate, and hence the introduction of cavitation nuclei, was held constant for all tests.

Figure 3-1 shows a typical set-up. [12] (Scale drawings of the horn can be found in Appendix D).

Figure 3-1 Vibracel Cup Horn Assembly

For the majority of tests Mr De Quieros followed a method of inserting a piece of aluminium foil to the sound field for a specified length of time (typically for 30

seconds), sonicating it, and then removing the foil for visual inspection of the cavitation damage. This was a substantial body of work and provided a base from which further experimentation could be conducted.

3.2 Foil Method

Cavitation fields are unfortunately extremely difficult to measure and analyse due to their chaotic nature and rapid variation. A method of taking a "long exposure image" of the cavitation field to effectively accumulate or average the region in which the cavitation is prevalent is needed. This foil technique of measuring the destructive ability of a particular cavitation field involves inserting a piece of aluminium foil into the cavitation field for a short time. The cavitation caused permanent damage to the foil, either totally destroying the foil, or partially damaging it causing it to appear pitted and bubbled. The foil unfortunately does disturb the sound field and for this reason the foil used must be extremely thin foil. (Section 1.1 contains references to other methods on cavitation measurement.)

3.3 Digital Image Processing

When analysing foil samples that were damaged or partially destroyed by ultrasonic cavitation, it was evident that an accurate, quantifiable means of analysing the foil samples was needed. Essentially what was required was a value representing the area of the foil that was destroyed or damaged. One of the best methods of doing this would be a digital image processor, as calculating these areas manually would be extremely time-consuming and error prone. The use of relative weight loss in the samples used in Heuter and Bolt [2] does not provide information about areas that were damaged, but only about the mass removed from the sample.

It was decided to use Matlab™'s digital image processing toolbox to calculate these values, as the language is easy to master and there are examples and help with similar

problems on the Internet. Although these programs are very powerful, it simplifies the programming to give the image processor data that can be easily manipulated, and for this reason the foil samples were placed with their dull side facing the digital image scanner, and using black paper as a backing. This black background was selected to ensure that there was an adequate intensity level difference between the intact foil, and areas that had been destroyed. The reason for facing the dull side of the foil up was because the flat sections of the shiny surface in the digital scanner would tend to come out very white or bright and distorted the images' intensity level gradients. In order to explain the process of extracting a value for the damaged, as well as the destroyed areas, as mask images and as a percentage of the total original foil area, an example will be used.

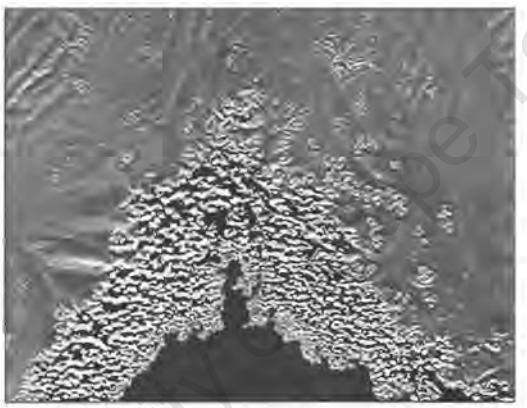

Figure 3-2 Original normalized image

Figure 3-2 shows a processed foil sample after scanning. The destroyed and damaged areas can be seen clearly.

3.3.1 Analysis and Extraction of Damaged Areas

In order to extract the damage areas, the program is required to generate a mask that covers the pitted foil yet excludes the black background and the smooth foil that is undamaged. The area of interest can be seen to contain rapidly varying intensities, which implies many local maxima and minima or edges in the intensity profile. A function that places a pixel at the position of each edge is used to get the following image shown in Figure 3-3.

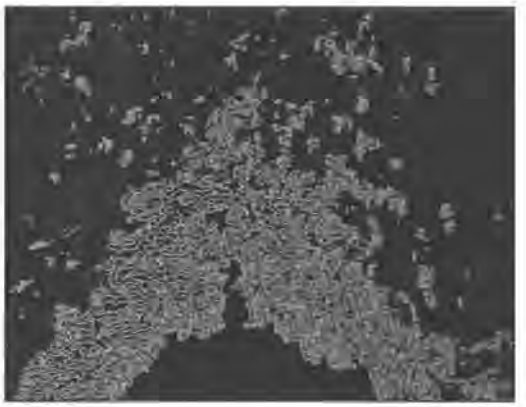

Figure 3-3 Edge Detected Image

This edge detection is extremely effective in finding the damaged area if one visually compares this image to the original in Figure 3-2; however the number of white pixels doesn't represent the damaged area. This can be corrected by filling in the regions between closely positioned pixels. Dilating each pixel and so grouping the pixels works well; however in that case the white areas exaggerate the damaged area. An erode function is employed to correct this exaggeration without ungrouping the pixels.

Figure 3-4 shows the final mask that represents the damaged area. It can be confirmed by detailed visual comparison that this gives an accurate mask of the damaged areas.

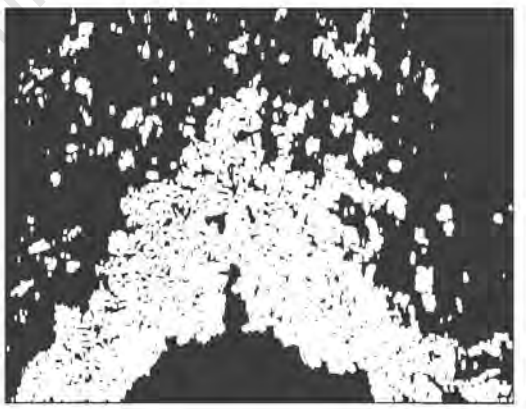

Figure 3-4 Final Damaged Foil Mask Image

3.3.2 *Analysis and Extraction of Destroyed Areas*

The extraction of the destroyed area is marginally easier than that of the damaged area. Once again starting with the normalized image in Figure 3-2, a mask needs to be generated that will represent the black background where the foil is destroyed only. An obvious solution is to carry out a threshold detection, which involves taking the intensities above the threshold value and setting them to 255 or white, and similarly setting those below the threshold value to 0 or black. A threshold value of 51 ensured that the entire black region was included and resulted in the threshold image in Figure 3-5.

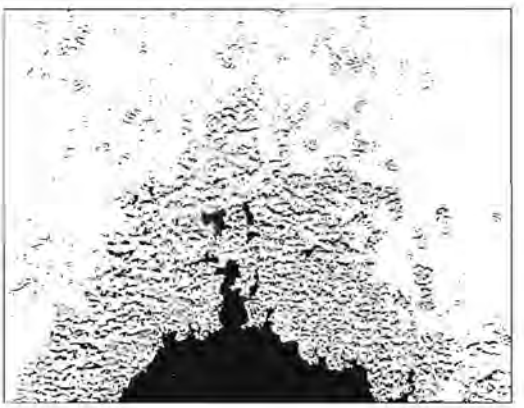

Figure 3-5 Threshold Image

This threshold image represents the entire destroyed area, but unfortunately it includes the dark areas of the damaged regions. This can, as before, be corrected by the grouping strategy explained in the previous section, however in this case the erode function was carried out first, and then the dilate function, because of the inverted colours. The result is the final destroyed mask shown in Figure 3-6 below.

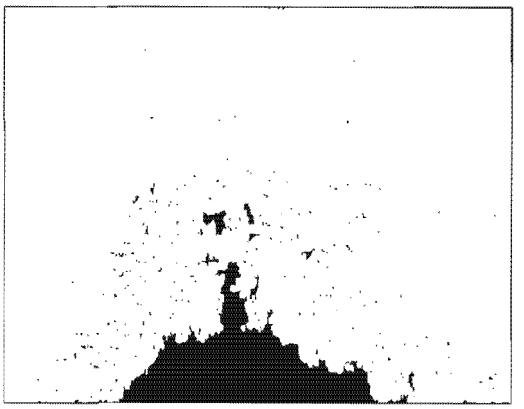

Figure 3-6 Final destroyed mask image

This final mask in Figure 3-6 appears to have quite a few outlier pixel groups, but on closer inspection the pixel groups do in fact represent smaller areas of destroyed foil. Other isolated pixels do represent errors in the method, but these cannot be reduced without altering the larger relevant areas. With this in mind, and the fact that these isolated pixels numbers are very small compared to the total number of pixels, this compromise was found to be acceptable.

For the above foil sample the damaged foil percentage is 31.15 % and the destroyed percentage is 7.95%. These were calculated by summing the pixels representing the damaged and destroyed areas and expressing them as a percentage of the total number of pixels. The image processor produces a reliable, reproducible and resource efficient method of analysing foil samples that have been damaged by a cavitation field. This method is not only attractive in terms of its speed, but also its flexibility that allows batches of samples to be processed unsupervised. [10] The complete code can be viewed in Appendix A.

3.3.3 Mean Deviation on Foil Samples

In the above description of the image processor one can clearly see that it produces accurate results with a near perfect repeatability on the same foil sample irrespective of scanning position. This was due to the methods reliance on pixel groups and not

individual pixels for calculations. All scans were done at the same resolution for consistency in the image processor. However, the errors in results obtained in this thesis reflect the inconsistency of the cavitation field, which is unfortunately rather chaotic. The errors obtained in the tests conducted in this thesis do not necessarily reflect a failure of the foil method but merely show the chaotic nature of the cavitation fields. Nonetheless, a measure of certainty needs to be established for the validation of results in the proceeding chapters. A series of test were done on foil samples under identical conditions to establish the standard deviation and give a range in which the results vary due to errors. It was found that this standard deviation was 0.08 of the total. This means that there was 69% certainty that a value of X would be in the range X ± X times by 0.08, as many of the foil sample tests were done in very similar experimental set-ups to the tests where the mean deviation was calculated.

3.4 Streaming

In order to measure the various parameters associated with, and influencing acoustic streaming, a method of visualizing the streaming patterns and recording these to be analysed was needed. There are various methods of doing this, using a wide variety of liquids, powders and dyes to visualise the streaming effects. In this project water-like solvents are primarily used, and for this reason it would make good sense to use water in the tests. Fine aluminium powder introduced into the water generates a dark cloud; this is then enhanced by placing a black surface behind the reaction vessel together with a backlight, giving a typical image shown in Figure 3-7. Fortunately, the reaction vessel was made of glass, making recording of the streaming patterns with a digital video camera effortless.

Figure 3-7 Streaming Pattern of Water visualized by Aluminium Powder Cloud

These 5-second MPEG movie clips were stepped through frame-by-frame to extract information such as the extent and velocity of the streaming patterns. (Appendix C shows a progression of the movie frame-by-frame).

3.5 Temperature Measurements

Temperature measurements for most of the project were taken with the use of a conventional laboratory thermometer. These are acceptable for static temperatures and will not be discussed further. However, the measurement of dynamic or time-varying temperatures such as those used in the temperature profiles need to be considered for their accuracy. These measurements are distorted in that the temperature probe (in this case a LM35 electronic thermal reference) has a small heat capacity, and hence there will be a time-lag between the real temperature and the measured temperature. This can be compensated for if the thermal system is expressed in terms of its electrical equivalent and the temperature probe is modelled as a low-pass filter. The actual temperature can then be calculated from the measured temperature. This is useful if a certain organic sample can be damaged at a particularly high temperature, because the real maximum temperature of the solvent can be accurately estimated from the measured temperature. (The exact method was explained more completely in the section entitled Thermal Shocking.)

4 Static Pressure

This chapter is concerned with the effects of static or atmospheric pressure on cavitation with reference to its strength, density, and ultimately its ability to disrupt solids. A number of tests needed to be carried out in an environment in which the static pressure of the water could be varied while still enabling an acoustic intensity sufficient to cause cavitation to be transmitted into the vessel. [2] This discussion consists of two parts: firstly, the design and construction of the pressure apparatus, together with comparisons between this new vessel and the original glass cup horn (used in previous tests including those done by Mr Ricardo de Quieros [12]); and secondly, a description of the tests and conclusions drawn from them.

4.1 Design of the Pressure Apparatus

In addition to the primary requirement of bearing the pressure, this new vessel had to be made of relatively lightweight material so as not to overload the transducer, yet strong enough to withstand up to two Bars of internal pressure and one Bar of external or negative pressure. The vessel needed to be constructed in such a way that the internal volume was easily accessible for checking and replacing of test samples etc. An important requirement that was not immediately obvious was that all the air needed to be removed from the vessel to ensure that degassed water would not 'breathe' while cavitating (i.e. absorb minute amounts of air into the water, allowing the water to cavitate more easily). It was also necessary to make provision for internal mechanical connections that were used to hold the test piece in place.

4.1.1 Design and Experimental Conditions

The first and most pressing concern was the seal around the horn and whether it would stand up to the high pressures involved. To simulate the glass cup's fixing point to the transducer a piece of steel tube was machined to the same shape as the glass cup. Another piece of steel was machined to the same shape as the plastic lug as shown in Figure 4-1. However, there was no thread on either of these new components, as this would have significantly increased the cost and time of machining. The method of tightening or compressing the rubber o-rings can be seen in Figure 4-2, where tapered slots in the PVC piping provided a primitive yet effective thread. This method of compressing the o-rings and fixing the vessel to the horn only work if the other socket was firmly fixed to the PVC piping. This was achieved by making the outer diameter of the component slightly larger than that of the pipe, giving an interference fit that was also glued for added strength.

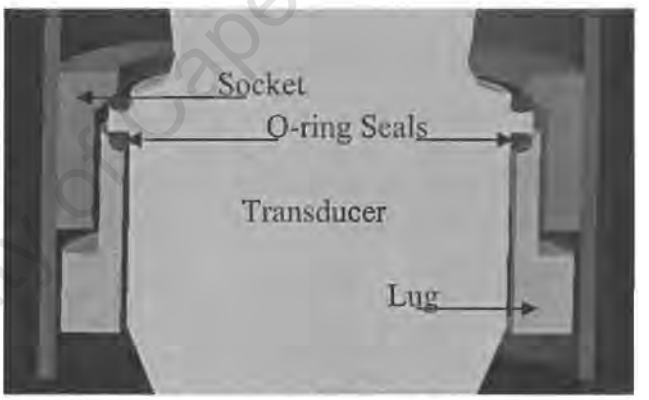

Figure 4-1 Pressure Apparatus Cross Section, showing the method of sealing the vessel.

The PVC piping was chosen because it was easy to work with, and has the added benefit of being a glue-on, off-the-shelf component that is able to handle the high pressures involved.

Figure 4-2 shows the grey plastic converter and the steel screw-in end cap. The 3mm nut and bolt internal connectors can be seen protruding from the grey converter. A scale drawing of the apparatus can be found in Appendix D.

Figure 4-2 Assembled Apparatus Showing the Assembled Apparatus

The pump used to pressurise the vessel was a hand pump rated at 30 Bar positive pressure and 5 Bar negative pressure, with a built in pressure sensor and digital display. (See Figure 4-3). Although the negative pressure was never a priority, this extra capability provided additional insight into the effect of static pressure on cavitation. As mentioned before, it was important that the water under pressurisation was not able to 'breathe' or be in contact with air during sonification. However, the pump only functioned in air, and for this reason the air/water separation reservoir needed to be constructed. This was simply a vessel that was half-full of water, with two connecting points, one at the top for the air or pump connection, and the other at the bottom for the wet or reaction vessel connection.

Figure 4-3 Pressure Pump

Ensuring that the cavitating liquid did not breathe also meant that sources of other dissolved gases needed to be limited. For this reason, distilled water was used as the coupling/cooling fluid. That, though, meant that the coupling fluid would get hot (up to 30˚C after a few 10 second tests). This was solved by replacing the coupling fluid with the same fluid but at a temperature of 23˚C. The transducer was then briefly turned on to allow any air trapped by the changing of the fluids to be released. This air was then vented, and the vessel was pressurised for the various tests. The liquid in the receptor vessel was also replaced to both ensure a constant temperature for each experiment as well as to clean the vessel of destroyed pieces of aluminium foil. As in other experiments, the receptor vessel was fixed 1mm above the emitting-face of the transducer to minimise acoustic absorption.

For measuring of power related data, the amplitude of the transducer was set on the Vibracel unit and the power was read off it (this was most likely electrical power and not exact acoustic power). Efforts were made to get the exact meaning of the power display from the manufacturers without success, but it was assumed that it could mean one of two things: electrical power or acoustic power multiplied by the efficiency of the transducer. Both of these quantities are sufficient for comparison purposes. Figure 4-4 shows the basic experimental arrangement.

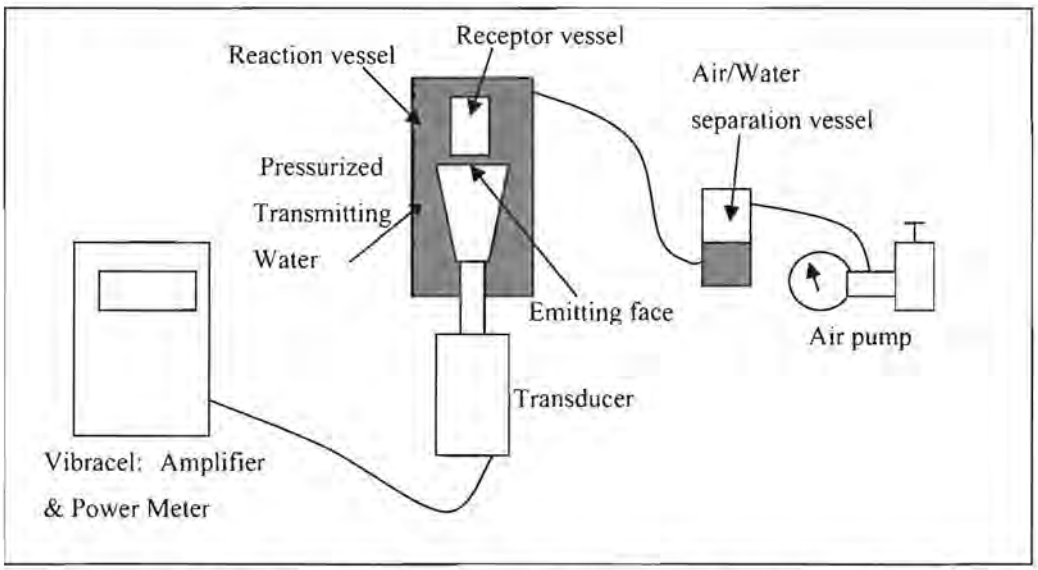

Figure 4-4 Pressure Tests Experimental Setup, Showing the Interconnection of the Pump and Pressure Vessel.

4.1.2 Plastic Bottle Sealing

The plastic bottles were sealed for reasons that will be explained later in this chapter. These bottles, once sealed, were required to withstand an external pressure of up to 1.5 Bars without allowing any water to seep or leak into the bottle. Various adhesives were tried without success, even for pressures as low as 0.5 Bar. The solution finally implemented was a technique found in the gas and oil industry for joining large plastic piping sections. [17] This involved winding a resistive wire around the lid of the bottle, closing it, and applying a large current through the winding causing it to heat up and melt the lid on to the rest of the bottle. The wire then remained inside the seal and the loose ends were trimmed. This provided an excellent seal that was extremely difficult to break open, even by hand after the tests for inspection of the foil sample.

Figure 4-5 Plastic Bottle being Sealed

4.1.3 Comparison between Glass and New Pressure Vessel

In order to compare the results obtained in the pressure vessel, with those of the glass vessel and with those of previous work done with the glass cup horn, a conversion factor or relationship between the two vessels needed to be experimentally obtained.

The first method of comparing the two vessels consisted of recording electrical power input (displayed by the Vibracel amplifier) into the transducer for various amplitudes. This would give a measure of the resistive force in the new vessel compared to that of the glass vessel, as the Vibracel adjusts its power to maintain a steady amplitude using current feedback. From the graph of Amplitude vs. Power in Graph 4-1 below, a slight power offset of 2.8 Watts can be seen between the two vessels, which could be explained by the fact that the pressure vessel was slightly heavier than the glass cup horn.

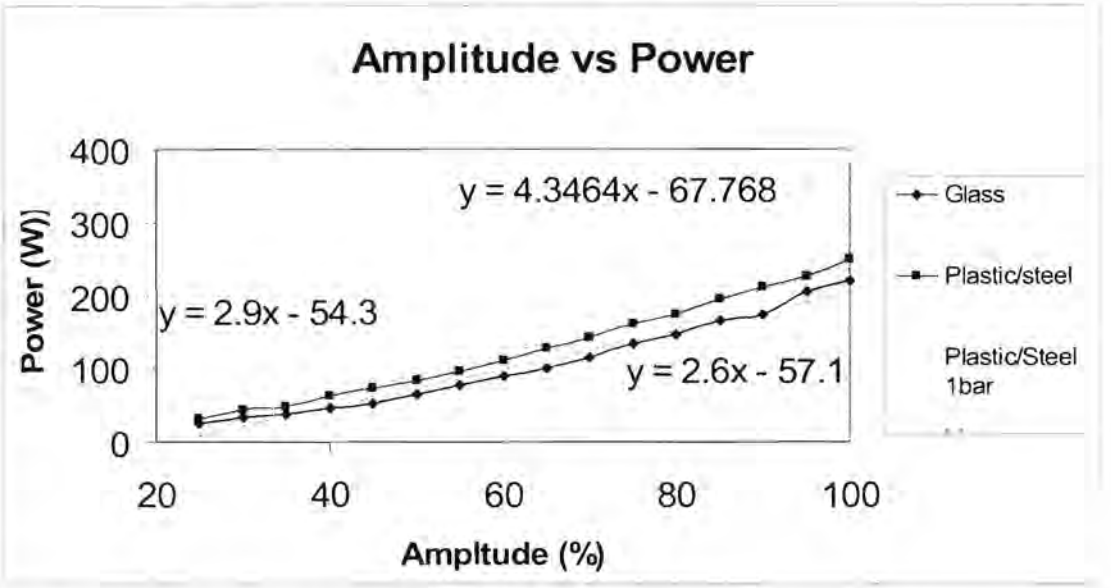

Graph 4-1 Amplitude vs Electrical Power, showing The Average Power Consumed over a Ten Second Period for Various Amplitude Settings for the Different Vessel.

It can also been noted from the linear trend lines fitted to the data series that the gradient for the pressure vessel is about 10% larger than that of the glass vessel. This may be because as the amplitude is increased the plastic approaches a non-linear region of its stress-strain curve, and it begins to absorb more energy.

It is also interesting to note the third (upper) data series in Graph 4-1 above, where the external pressure was increased to 1 Bar and the power at 100% amplitude subsequently doubled. As an increasing power implies an increasing destructive capability, this was a very positive and exciting result.

While the amplitude-power relationship between the two vessels gives a reasonable comparison in terms of the electrical energy used, it was also necessary to conduct some tests that compared the destructive capabilities of the two vessels, as this was one of the goals of this research. As a result, a series of tests was conducted, again using the foil method. This time, however, the foil was placed directly into the vessel without first being inserted into a bottle. Tests were done under open or atmospheric conditions for both the vessels, using degassed water at the same temperatures (23°C) and heights above the transducer (35mm) and subsequently very similar volumes of

water. The idea was to set all conditions to be identical to ensure that the results would only reflect differences between the two vessels.

The amounts of damaged and destroyed foil were calculated with the Matlab™ based image processor. A disruption index was calculated using a weighted sum of these two values (weighted 1:2) to place an emphasis on the value representing the area of destroyed foil (as this area represents greater destructive forces). These two disruptive indexes were compared firstly as a function of amplitude, and then as a function of power. This revealed that the pressure vessel at similar amplitudes produced 74.8% ± 2.9% of the disruption of the glass vessel, and at similar power levels the pressure vessel produced 63 % ± 2.5 % of the disruption of the glass vessel. This implies that the new pressure vessel is 63%± 2.5% as efficient as the glass vessel. Again, this was most likely due to the fact that the pressure vessel was heavier, and consisted of more lossy material than glass. This was not a problem as long as the inefficiency or conversion factor between the glass cup's horn and the pressure vessel was kept in mind when comparing results.

4.2 Pressure Effects on Transducer

Varying the static pressure of a liquid under high power sound waves significantly affects the cavitation strength and bubble size, as well as the load that the transducer has to drive. This section investigates the effects of static pressure variation on the transducer and the way in which it responds.

4.2.1 Pressure Effect on Power

In Graph 4-2 of Pressure vs. Power, the power (This was average power over 10 seconds) required to drive the transducer was recorded while increasing the pressure. This once again showed that the increase in pressure results in a higher power being required to maintain specific amplitudes: in this case, at a 50% amplitude setting.

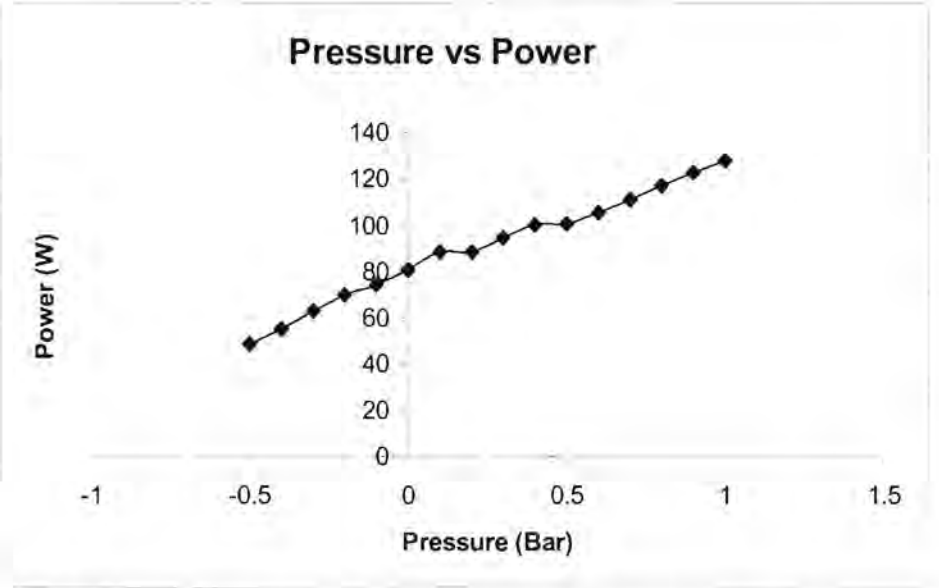

Graph 4-2 Power Variation with Pressure where The Pressure was expressed as Differential Pressure where 0 Bar is Atmospheric Pressure.

By increasing the static pressure one increases the cavitation threshold pressure, subsequently suppressing the cavitation as implied by

Equation 2-1. Cavitation has the effect of unloading the transducer because of the compressibility of the cavitation bubbles and the energy being dissipated throughout the liquid by the heating and shockwave effects of the cavitation. It was therefore evident that an increased static pressure would mean an increased load and therefore an increase in the power required to drive the transducer.

4.2.2 Pressure Effect on Resonant Frequency

In addition to the power changing in response to pressure, a frequency change was also noticed for different pressures. Graph 4-3 below shows how the Vibracel unit tracked the resonant frequency as the pressures increased. This change in resonant frequency was most likely due to the resistive forces increasing, from a reduction in cavitation (i.e. transducer, vessel, water and cavitation bubbles) as a result of pressurising.

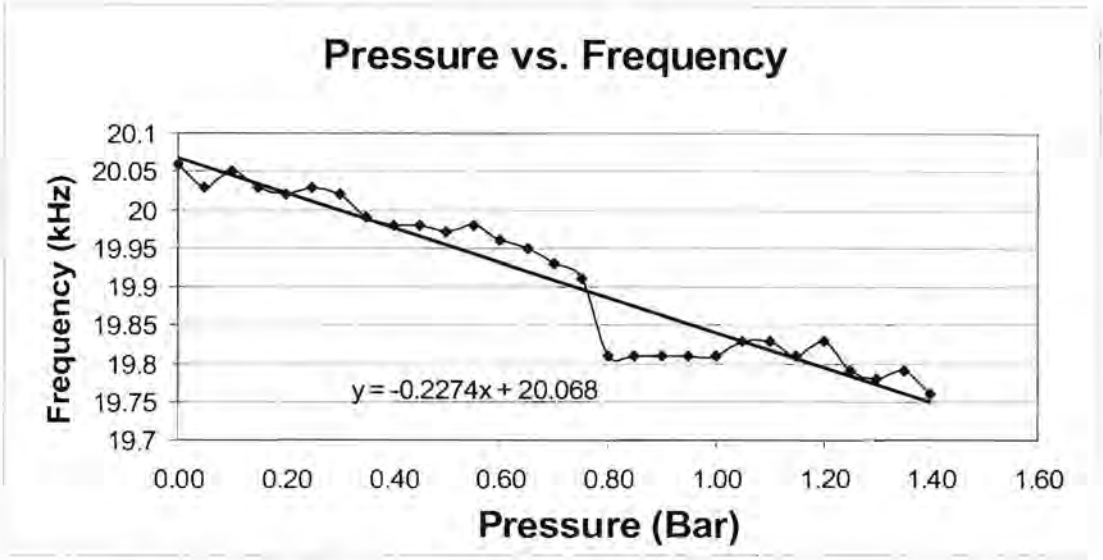

Graph 4-3 Pressure vs. Frequency, Showing the Drop in Frequency as Differential Pressure was Increased.

Although the frequency variation is less than 1.5 % over a 1.4 Bar range, the Q of most transducers, (including this one) is high, reiterating the need for a PLL (Phase Lock Loop) to track the resonate frequency. Fortunately a PLL was included in the Vibracel amplifier.

4.3 Static Pressure Effect on Disruption

Once again the foil test was used to establish the disruptive capabilities of cavitation. This time, however, the pressure was varied in order to find the static pressure that produced the most damaging cavitation in water. This test was initially done over a broad range with a resolution of 1 Bar. Once the general area in which the highest cavitation occurred was found, more accurate tests with a resolution of 0.1 Bar were done to establish the exact optimised pressure.

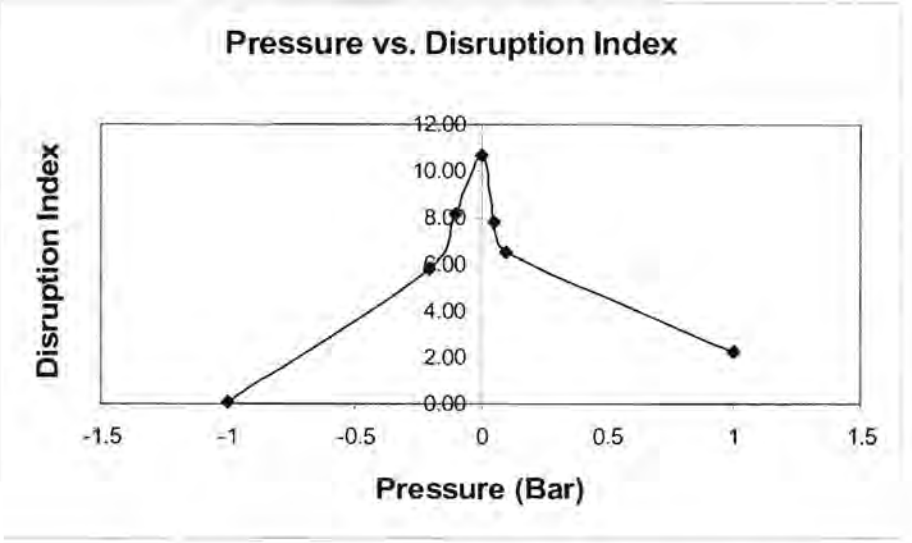

Graph 4-4 Disruption as a Function of Static Pressure

These results are shown in Graph 4-4 where, unfortunately, the optimised pressure was in fact atmospheric, which would indicate that all the tests done so far at atmospheric conditions were in fact carried out using an optimised static pressure and no additional destructive capability can be achieved by varying the static pressure.

However, if one looks at the reason for the lack of disruptive cavitation at -1 and 1 Bar, for example, the reasons are distinctly different. In the case of -1 Bar the static pressure was reduced so much that the high intensity sound waves cause cavitation bubbles to form but not to collapse violently; instead, they bubbled to the surface (audible bubbling was heard). On the other hand, at +1 Bar the formation of the bubble seemed to be suppressed, correlating with Hueter & Bolt's findings set out in Chapter 2. [2] This implies that there is little or no cavitation to scatter the sound field or sound waves. This effect could be harnessed if one could pressurise the transmitting medium to reduce or eliminate cavitation and have the solvent or disrupting liquid at atmospheric pressure. This would, in effect, localise the cavitation in the area where it was needed. This was the reason for sealing the plastic bottles in an effort to maintain the pressure difference.

4.4 Differential Pressure Testing

This section sets out to prove and optimise the previously explained principal of using a differential pressure to increase and localise the cavitation in the receptor vessel. Once again, all the factors affecting cavitation were set constant, so that the results would reflect only the changes in differential pressure. Tests were done, all with the internal pressure at atmospheric pressure, as this had already been found to be the optimum pressure for the most destructive cavitation. The pressure for the transmitting medium was then varied from 0 through to 0.75 Bar gauge pressure. Foil samples and image processing were again used to quantify the amount of disruption; the results are shown in Table 4-1 below.

Pressure ratio	% Destroyed	% Damaged	Disruption Index
0 / 0	1.88	26.10	9.95 ± 0.795
0 / 0.25	13.73	19.63	15.70 ± 1.26
0 / 0.75	24.63	19.75	23.00 ± 1.84

Table 4-1 Differential Pressure Results

This revealed some very positive results where the theory above was confirmed, and the percentage damage was increased by 2.5 times from 0/0 to 0/0.75 (receptacle pressure/external pressure).

4.4.1 Effects of Water Level Variations

The effects of the water level variations in the receptacle were once again quantified using the foil and image processor technique to give the results in Table 4-2. It is apparent from Table 4-2 that a water level (inside the receptor) of 20mm gives the maximum disruption by a significant margin. This is most likely due to the fact there is a small volume being subjected to ultrasound, creating high-density high energy levels. The reason for a water level of 10mm not having a higher disruption index could be explained by the small contact surface area, and a liquid level being too low

to create standing waves. The 20mm level simply constitutes an optimal operating point between the two effects, and thus results in the most destructive cavitation.

Water level	% Destroyed	% Damaged	Disruption Index
10mm	32.02	11.32	25.12 ± 2
20mm	57.39	10.29	41.69 ± 3.3
30mm	11.64	28.90	17.40 ± 1.3
40mm	4.69	20.65	10.01 ± 0.8

Table 4-2 Disruption as a Function of Receptacle Water Level

4.5 Conclusion

The effects of pressure or, more specifically, the effects of differential pressure, have obvious advantages in terms of a disruption system. On the other hand, the time taken to complete a single pressure differential experiment was well over twenty minutes due to the complex mechanisms that provide the seals for these relatively high pressures. Although the differential pressure has obvious benefits, it also provides significant complications and, as a result, increased costs of making a system that would include this differential pressure technique.

5 Tri-Reactor Vessel

In the previous chapter, the sound intensity transmitted to the receptacle was increased with an increase in static pressure; however, this method was time-consuming and complex. This chapter will consider a second method of transmitting increased acoustic intensity to the receptacle. This method involves the use of multiple transducers in an ultrasonic bath set-up. In an attempt to overcome the saturation effect when the most acoustic energy was transmitted through a single path to the receptacle, three transducers were fixed to a triangular bath (hence the Tri–Reactor name) and a variety of receptacles, including a triangular prism vessel, were tested in this new bath. In the interests of completeness, the effect of static pressure on the multiple transducer baths was also measured to confirm the results of the previous chapter. Finally, a comparison between this new vessel and the 500 Watt Vibracel (in terms of power and its destructive capability) as well as its ability to process biological samples was discussed.

5.1 Experimental Apparatus

The apparatus for this chapter varied from the rest of this project primarily in terms of the method of driving the transducers. Figure 5-1 shows the basic layout of equipment, the signal generator, amplifier, transformer and power meter. The transformer was used to increase the voltage of the amplifier to enable the transducers to work efficiently and the amplifier to be loaded with the correct impedance. Once again, the receptacle, bath, and transducers were cooled by circulation of the cooling liquid (23°C), which also acted as the transmission medium. The rate of flow of cooling water was 250ml /min.

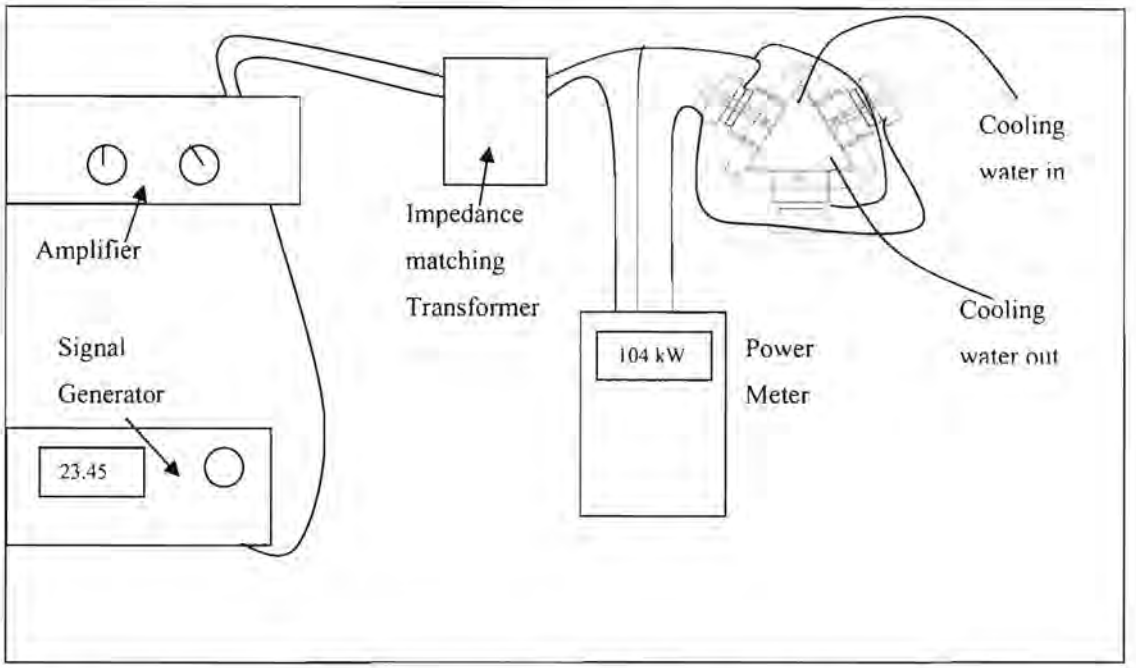

Figure 5-1 Experimental Set-up, Showing the Tri-Reactor and its Electrical Connections to the Power Meter and Amplifier

5.2 Design and Construction

5.2.1 Geometry

The design requirements were that a number of transducers needed to act on a volume of liquid as small as possible; however, each transducer needed to be mounted on a 100x100mm stainless steel plate to enable the chosen square transducer to resonate adequately. The obvious choice would be to use two transducers facing one another in a bath that has a rectangle shape in the top view; however, this was avoided because of multimode resonance being set up between the two transducers. The next option was to construct a triangular prism bath and use three transducers, one on each of the triangular faces. The advantage of the equilateral triangular shape was that it has a higher surface area to volume ratio than other regular polygons of a higher order. As a result, a triangular prism with sides of 100mm by 100mm was constructed from stainless steel (to reduce pitting under heavy cavitation). To further

secure the bond of the glue that couples the transducer to the bath, threaded studs were welded to the bath's walls to provide a screw-on fixing point for the transducers. In order to facilitate pressurising, the wall thickness of the triangular bath was set to 2.1mm. This was slightly above the manufacturer's recommended thickness for the mounting plate of a transducer, thus a resistance against the plate flexing too much under pressure was required and a compromise was made. In addition to this, a flange, lid and rubber seal were constructed that could handle pressure in excess of 2 Bar.

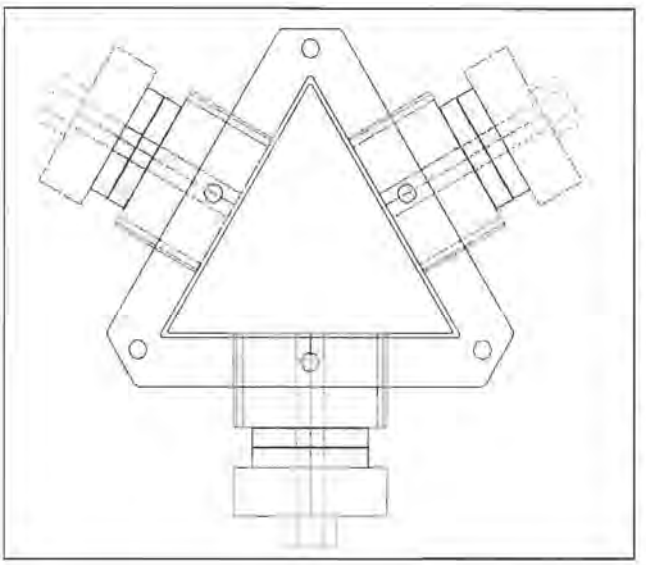

Figure 5-2 Top view of Tri-reactor, Showing a Top View of the Bath and Three Transducers (Dimensioned drawing in Appendix D).

The transducers used were designed by MP Interconsulting, Switzerland, using PZT-8 or better quality, piezoceramic material with aircraft grade aluminium and a centre bolt. Figure 2-8 shows an exploded view of the transducer where the two sandwiched PZT disks and their orientation can clearly be seen. Detailed scaled drawings of both the transducer and the triangular bath can be found in Appendix D.

5.2.2 Transducer Selection

The transducer selection was critical in terms of resonant frequency, and the impedance characteristics at that resonant frequency, as it would simplify the system greatly to have all three transducers running at the same frequency on the same amplifier and, if possible, in parallel. Fortunately, a number of these square transducers were available for testing. The impedance characteristic as a function of frequency was attained using a network analyser. The resonant frequencies and their associated maximum conductance (G) were graphed for easy visual selection of similar transducers.

Graph 5-1 shows the three transducers selected. (Two were in precisely the same location.) The transducers individual characteristics (G & B traces) are given in Appendix B.

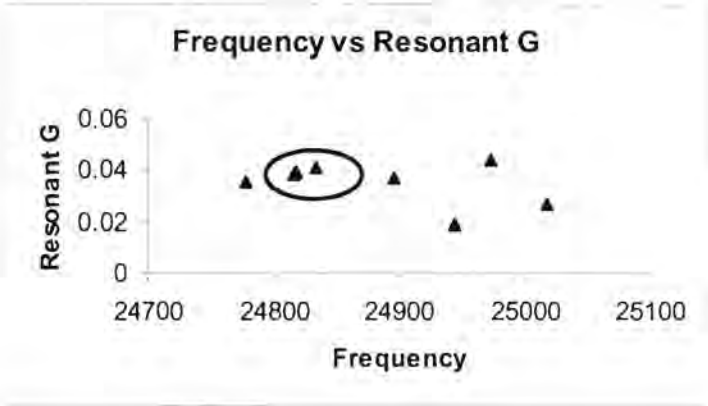

Graph 5-1 Transducers Resonant Frequency Characteristics, Showing Selected Transducers.

5.2.3 Resonance Modes

In order to drive the transducers at maximum power, the driving frequency needs to be the same as the resonant frequency. Graph 5-2 shows a conductance (G) and admittance (B) trace as a function of frequency. It can be seen that there are a number of minor resonance points (as in any real system) and a major or dominating resonance at about 23.190 kHz. Unfortunately, the resonance characteristics change significantly under load (and the load varies for different power levels due to cavitation). It was necessary to keep the transducer in its dominant resonant frequency during operation. This was done with the aid a variable frequency source, power analyser and an oscilloscope. The frequency was continually adjusted to ensure a constant phase between voltage and current as well as a constant power. However, in a commercial unit an electronic tuning circuit such as a PLL (Phase Lock Loop) would be needed.

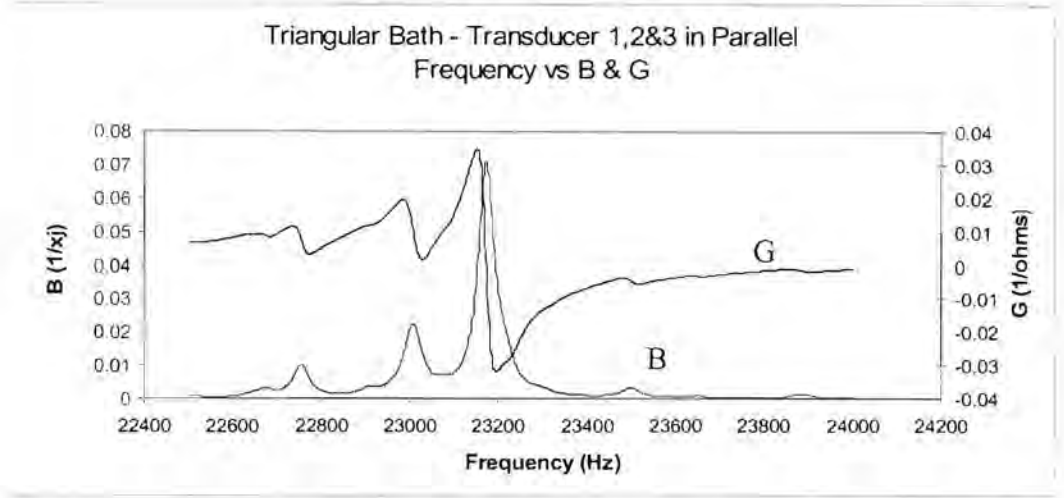

Graph 5-2 Frequency vs. G & B

Using Graph 5-2 and the graph of the unloaded system it was possible to calculate the electromechanical efficiency using the following equation:

$$\eta_{ma} = \frac{G_{air} - G_{load}}{G_{air}}$$ **Equation 2-29**

This gave an efficiency of 89%. However, this value did not apply to the system under load and at high power; it only gave an estimation of the efficiency. The loading condition was with the vessel filled with water, and the unloaded values were taken while the vessel was empty with the aid of a network analyser. Graph 5-3 shows the dynamic impedance as the power was increased, all the time ensuring that the system was in maximum resonance by tuning the frequency appropriately.

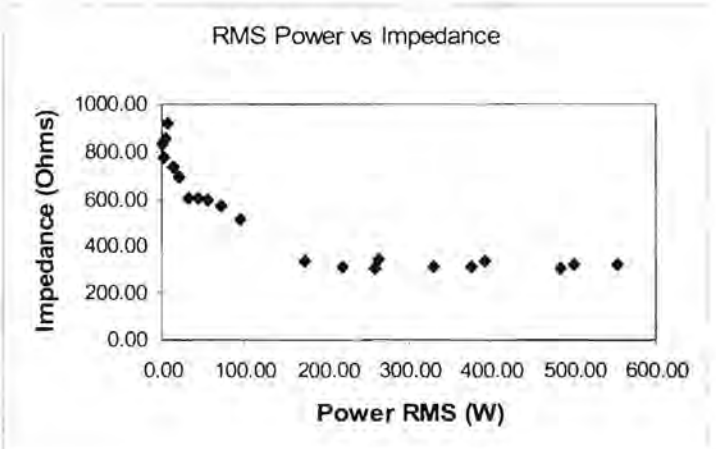

Graph 5-3 Dynamic Impedance of all Three Transducers in parallel as a Function of Power

It was evident that the transducer electrical-mechanical characteristics vary considerably under load, further enforcing the need for electronic control in a commercial unit for both frequency and power.

5.3 Mapping the Sound Field

Before tests with receptacles could begin, an idea of the sound field and focal points needed to be established. Once again, foil samples were inserted into the vessel and subjected to ultrasonic radiation. The foil samples were secured on a plastic and wire rig at various levels throughout the bath. These foil samples were then scanned and process in Matlab™ to give images below, where the black areas show the destroyed foil and the grey areas the damaged foil.

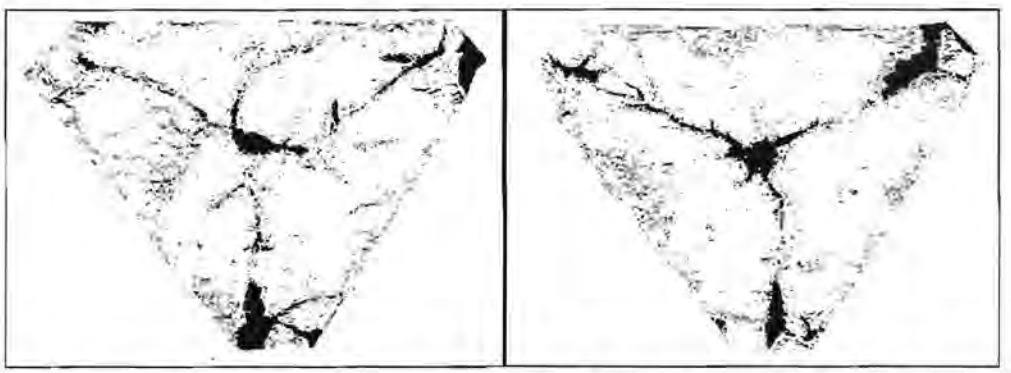

Figure 5-3 Cavitation Field Cross-section for 40 & 50 mm Above the Base, Showing the areas of Cavitation Damage and Advantages of the Digital Image Processor.

5.3.1 Focusing

Figure 5-3 above shows the areas of damage on the foil samples placed midway up the bath (on the centre line of the transducer). This was the level at which the most disruption occurred and areas of high cavitation intensity can be seen clearly. It is evident from these images that there is a large amount of focusing and as a result destructive energy at the centre of the triangle. This makes intuitive sense in that the three ultrasonic waves all converge at this point, and because the waves are in phase

due to all the transducers being in phase, the amplitudes of the waves are added by the principal of superposition to create an intensity level in theory roughly three times the surrounding area. In addition to the central focal point, lines can be seen running from the centre to the corners of the triangle. This can be explained in much the same way, however it is less dramatic because now only two of the waves are in phase along these lines. If one of the transducers is switched off, it can be seen that the lines from the centre to the corners are created by the two transducers closest to the line as shown in Figure 5-4.

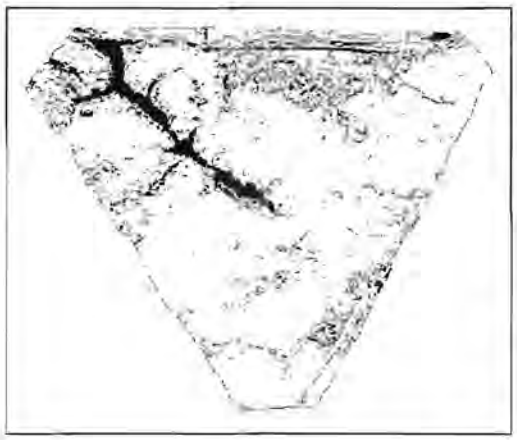

Figure 5-4 Focusing of Two Transducers, where the upper and lower left transducers were active and the right transducer was off.

5.4 Optimising the Receptacle

In order to compare this new reactor vessel with previously used equipment it was necessary to optimise the disruption in this particular set-up. This was done with a series of receptacles of various sizes, shapes, materials and volume levels. It was obvious from the mapping of the sound field that the centre of the vessel is the region with the highest sound intensities, and for this reason all receptacles will be placed in the centre and at a height that would insure that the centre of the solvent volume is subjected to the most intense radiation. From the previous section this was found to be mid way up the bath, along the centre line of the transducers. The following tests were done in a similar way to the other foil based tests in this project by placing the foil vertically orientated in the receptacle and sonicating for five seconds. The receptacles were once again made of polypropylene.

5.4.1 Effects of Multiple Transducer on Receptacle Disruption

The first test done was to establish the effect of having multiple transducers sonicating a full 50ml receptacle. In the graph below a clear improvement can be seen with an increased number of active transducers, while the electrical power driving the vessel for all combinations of transducers remained constant at 120 Watts. Although electrical power is not directly converted to acoustic power, it was assumed that the efficiency for the three transducers was very similar.

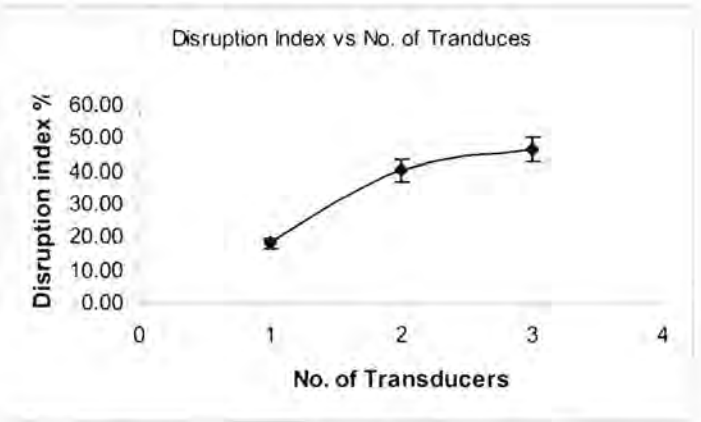

Graph 5-4 Effect of Multiple Transducers

This increase in disruption shown in Graph 5-4 was most likely due to the troublesome saturation effects being overcome with the three transducer design. The saturation effect is where the transmitting medium begins to cavitate and scatter sound energy, resulting in less power being transmitted into the receptacle. The effect of introducing more transducers increases the number of paths and the surface area that is transmitting acoustic power into the receptacle, thus increasing power intensity in the receptacle. Now with three transducers on, the saturation effect can be seen in Graph 5-5 below, where the power being transmitted into the reactor vessel is plotted against the disruption on foil samples placed inside the receptacle. A rapid increase can be seen in disruption from 0 to 100 Watts, however after that the disruption seems to saturate and even taper off slightly. This is most likely due to the fact that as the power increases the transmitting medium cavitates and these cavitation bubbles

absorb and scatter much of the sound energy as found in the chapter on static pressure. [2]

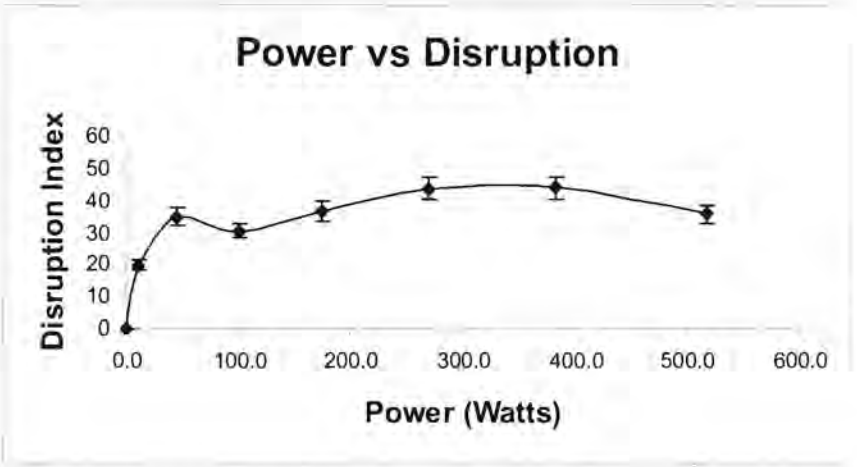

Graph 5-5 Disruption as a Function of Power, where the Saturation can Clearly be seen, the Disruption Levels off and Becomes Less as the Power is Increased.

5.4.2 Plastic Receptacles

In this test electrical power being delivered to the vessel remains constant, as well as fixing any other factors that could influence disruption such as temperature, geometry, receptacle position, etc. Various sizes of bottle and volume of solvent were tried, and the results are shown in the table below. The disruptive index per unit volume is of particular interest as this shows a measure of the sound intensity per unit volume of the solvent.

Bottle (ml)	Solvent level (ml)	Destroyed Foil %	Damaged Foil %	Disruption index per unit volume
10	5	4.7	24.6	13.6 ± 1.08
10	10	8.7	59.8	7.7 ± 0.61
20	10	0.1	13.6	2.8 ± 0.22
20	20	9.2	43.0	3.1 ± 0.24
30	10	1.3	15.0	5.3 ± 0.42
30	30	5.6	51.5	2.1 ± 0.16
50	10	0.2	13.3	6.8 ± 0.54
50	20	1.6	22.8	3.2 ± 0.25
50	50	10.1	36.0	1.1 ± 0.09
100	30	0.8	10.7	1.4 ± 0.01
100	100	8.2	45.3	0.6 ± 0.04

Table 5-1 Disruption Results for Plastic Bottles

From the Table 5-1, it can be seen that the small bottles with low volumes produced the most disruption as was expected; however when considering the disruption of organic materials, solvent saturation needs to be taken into consideration. This could mean that higher volumes of solvent would need to be used, and a compromise will need to be made between the disruptive force required and the amounts of solvent needed to fully dissolve the organic compound (a decision made by the end user).

5.4.3 Receptacle material

The glass receptacle tests were carried out in exactly the same manner as the plastic and although very similar trends can be seen, confirming the small bottle, low volume recommendation, the disruption is significantly lower when compared to that associated with the plastic bottles. This confirms conclusions made by Mr. De Quieros [12] and the theory of sound transmission through solid/liquid interfaces that glass is a poor material for use in this context. (Graph 5-6 shows a theoretical calculation of the sound transmission from water through the glass/plastic to water

based on Equation 2-9, where the transmission axis is a sound intensity percentage of an original 100%). The amount reflected at a material boundary is calculated with the acoustic impedance, which is the product of the density and speed of sound in the material.

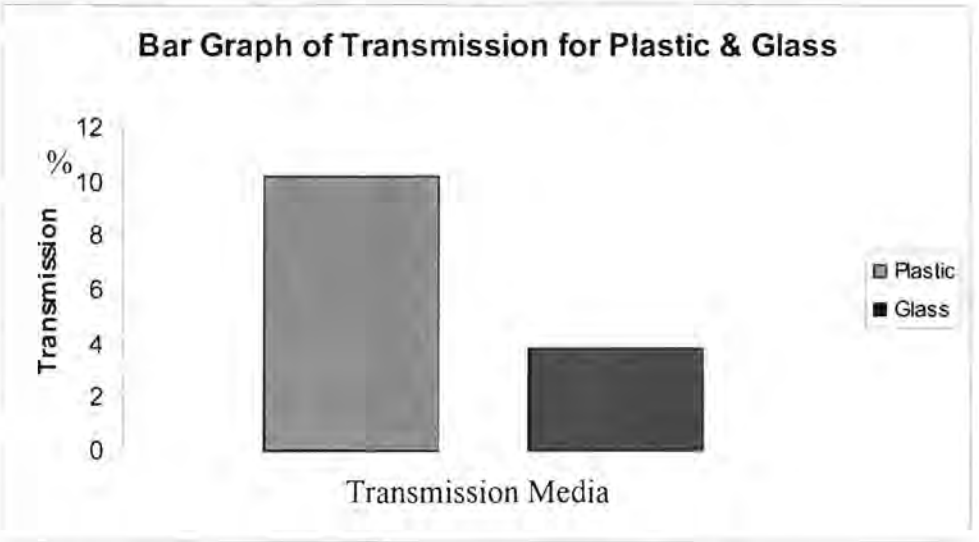

Graph 5-6 Theoretical Transmission for Plastic and Glass, Showing the Benefits of using Plastic over Glass.

Bottle (ml)	Solvent level (ml)	Destroyed Foil %	Damaged Foil %	Disruption index per unit volume
10.00	5.00	0.13	14.4	5.9 ± 0.4
10.00	10.00	3.15	36.4	4.3 ± 0.3
20.00	10.00	0.07	14.5	2.9 ± 0.2
20.00	15.00	2.5	13.6	1.7 ± 0.1
20.00	20.00	2.99	13.8	1.0 ± 0.1

Table 5-2 Disruption Results for Glass Bottles, When Compared to the Disruption Results for the Plastic Bottle it was Clear that Glass was Inferior, however Similar Trends can be seen.

5.4.4 Streaming

The method of measuring the streaming was the same as explained in Chapter 7, using fine aluminium powder suspended in water. Unfortunately, the acoustic streaming, which was critical to the mixing and ultimately dispersion, was not evident in the bottles placed in the tri-reactor vessel. It was already evident from previous tests that there was sufficient acoustic intensity in the bottle (enough to cause cavitation) so a low acoustic intensity could not be given as a reason for the lack of streaming. It was most likely due to balanced *radiation pressures* by the equilateral triangle arrangement that the streaming was suppressed.

5.4.5 Triangular Vessel Receptacle

In order to gauge the effect of a flat transmission surface vs. rounded transmission surface, a triangular prism receptacle and a cylindrical receptacle were constructed out of the same plastic. Figure 5-5 shows the damage on foil samples placed vertically in the cylindrical receptor vessel. These two images at different power settings show (in contrast to Figure 5-6) the apparent focusing effect in the cylindrical bottles very well. This focusing was most likely due to a cylindrical resonance set-up in the bottle walls by the three in-phase transducers, and not by lens focusing as initially thought.

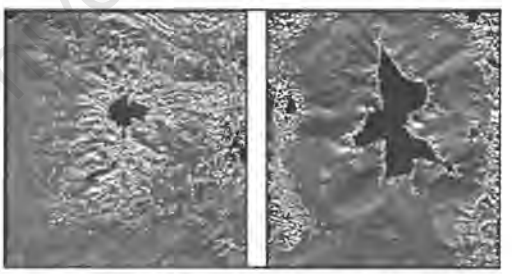

Figure 5-5 Foil Samples from Cylindrical Vessel

Figure 5-6 Foil Sample from Triangular Vessel

5.5 Pressurizing

To confirm the results found in Chapter 4 on Static Pressure, tests on both the apparatus and whether the cavitation was suppressed by the static pressure increase were carried out. Firstly, tests were done on the apparatus to gauge the effects of static pressure on the resonance frequency and power. These results were found to confirm those in Chapter 4 and are discussed below.

5.5.1 Pressure Effects on Resonant Frequency

The resonance frequency once again dropped slightly with an increase in pressure, shown in Graph 5-7, which again shows a linear trend. However, it must be noted that the gradient was double that obtained with the Vibracel unit.

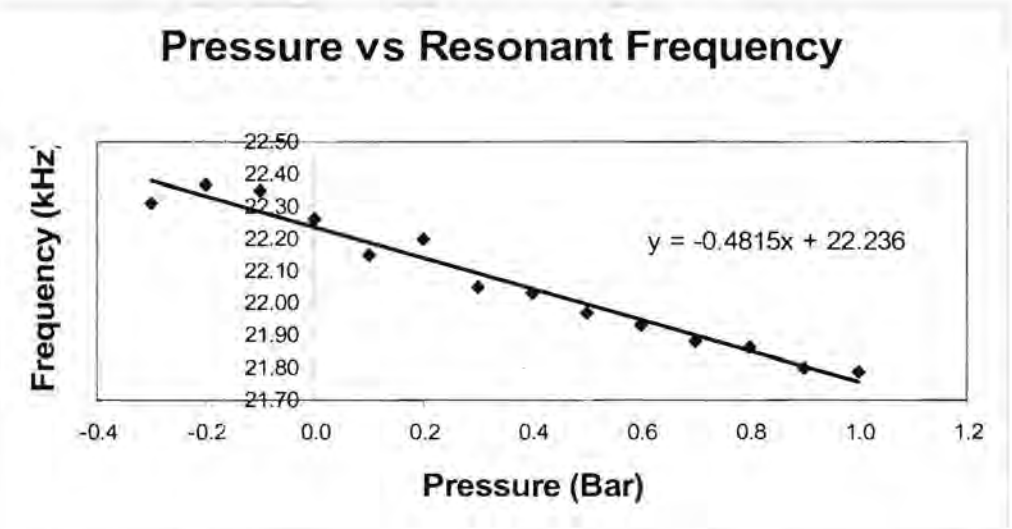

Graph 5-7 Graph of Pressure vs. Resonant Frequency, Showing the Frequency Decreasing with an Increase of Differential Pressure

5.5.2 *Pressure Effects on Power*

In Graph 5-8 below shows the triangular bath electrical power as a function of pressure. Although similar to the Vibracel unit in that power increased with an increase in pressure, the increase was remarkably less when compared to the same increases in pressure in the Vibracel. This was due to the different methods in which the transducers are controlled. The transducers in the triangular bath were simply driven at a constant voltage, which in contrast to the Vibracel unit involves no active feedback. The Vibracel unit uses a method of current feedback, presumably to maintain near constant amplitude on the tip of the transducer. This results in the Vibracel unit delivering more power to the transducer when under load (i.e. static pressure) to ensure that the amplitude on the transducer remains constant.

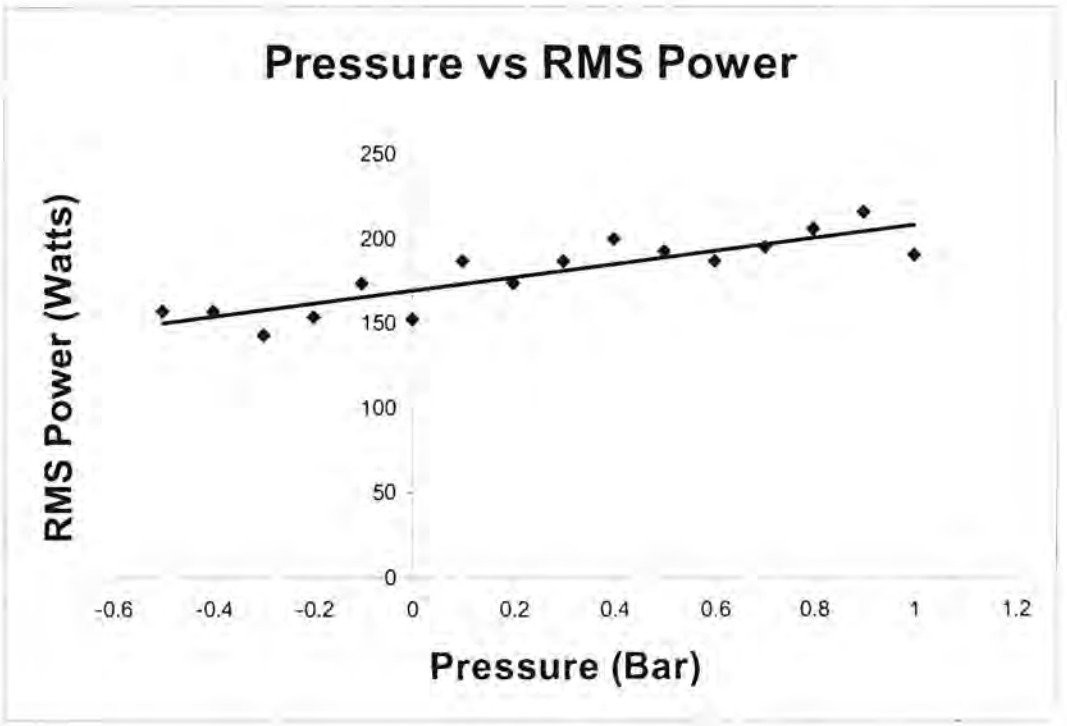

Graph 5-8 RMS Electrical Power as a Function of Pressure, where the Power Increases Slightly with an Increase of Differential Pressure.

5.5.3 *Differential Pressure Effects*

Tests similar to those in Chapter 4 using differential pressure were carried out on this triangular reactor vessel. Although the values in Table 5.3 below cannot be directly compared with those in Chapter 4, the ratio of any of the weighted sums over it's 0/0 differential pressure disruption index can enable a comparison with those in Chapter 4. It was found that although the pressure did increase the disruption, the increase of differential pressure was roughly 3/5ths as effective in the triangular reactor vessel as it was in the Vibracel unit. This could be due to two possible factors: firstly, the use of three transducers in overcoming the problematic saturation effect in the transmitting medium rendering the static pressure less effective; and secondly, the previously mentioned lack of feedback control and resulting relative power in the triangular vessel when compared to the Vibracel unit as the pressure was increased.

Pressure	Destroyed foil %	Damaged foil %	Disruption Index
0/0	7.5	38.5	17.8 ± 1.4
0/0.25	5.8	48.6	20.0 ± 1.6
0/0.5	6.9	60.7	24.8 ± 1.9
0/0.75	13.7	40.9	22.8 ± 1.7

Table 5-3 Differential Pressure Results

5.6 Comparison between Tri-reactor and Vibracel Unit

In order to gauge the differences and make a comparison between the tri-reactor and the Vibracel unit, three quantities or effects were compared. Firstly, simply looking at the electrical power being introduced into the system gives us an idea of effectiveness of the transducer. However this is extremely inaccurate as there are many inefficiencies in the transmission of ultrasound to the receptacle in both the transducers. The second method somewhat overcomes this problem by looking at the disruption within the receptor vessel (which is common to both arrangements) and comparing the power at which the disruption saturates, a high power indicating a better design in terms of delivering disruptive power to the receptacle. The third is simply comparing the vessels in terms of how the end product is intended to function i.e. its ability to disperse the organic solids.

When comparing the tri-reactor vessel which was driven at 550 Watts (max. at 0 Bar) and the Vibracel unit driven at 190 Watts (max. at 0 Bar) it implies that the tri-reactor vessel has a large advantage over the Vibracel unit due to the tri-reactor delivering more power.

Looking at Graph 5-5 the disruption as function of power reaching a maximum at roughly 300 Watts can clearly be seen; however it reaches 80% of the saturation value at 50 Watts. When comparing this to the Vibracel unit where the disruption saturates at about 100 Watts and reaches 80% of its reaching a maximum value at just over 40 Watts, it can be deduced that the tri-reactor vessel is more effective at delivering power to the receptacle.

5.7 Conclusion

The saturation problem was overcome, which was one of the main reasons for the construction of this multiple transducer bath. Based on the findings, it was evident that the use of multiple transducers increased the transmission to the vessel by about threefold. The effects of static pressure were confirmed on both the apparatus and cavitating liquid, and the advantages of differential pressure were shown once again. It was also recommend that a PLL be used in a final product to control frequency and, hence, the systems power. The tri-reactor can unfortunately not be recommended for a disruption cell as its tendency to suppress streaming caused the system to be ineffective. However, if a fourth transducer was placed at the bottom of the bath it could possibly unbalance the radiation pressures and result in streaming.

6 Transmission Media

This chapter considers the use of various liquids as a medium for the transmission of high power ultrasound to the treatment vessel. The goal was to reduce the attenuation in the transmission medium by some other means than the use of the time-consuming static pressure method. This chapter begins with a look at acoustic attenuation, due firstly to sound waves being reflected at material boundaries in theory, and secondly, to the effects of cavitation absorbing and scattering the sound energy in the actual system. This was followed by a series of tests showing the effect of using a broad cross section of different liquids as transmission media. The media were discussed in terms of the attenuation of the sound travelling through them and an optimum solution for a transmission medium was found.

6.1 Acoustic Attenuation

As already mentioned, the attenuation was believed to come from two main sources: the scattering effect of cavitation, and reflection at material boundaries. However, there is a third source of attenuation, namely the viscous losses. This needs to be taken into account when considering oils as transmission media that have significantly higher viscosity than water or water-based solutions. [2]

6.1.1 Theoretical Transmission Calculations

If one looks at the calculation for sound transmission through a material interface, it involves the two media's acoustic impedances. It is quite simple to maximise the transmission by making the two media's impedances as similar as possible. However, in a system where there are multiple material boundaries in series, the problem becomes more complex. This was further complicated by the fact that certain materials cannot be altered, such as the titanium face of the transducer, and the solvent (usually water or something of similar impedance). Graph 6-1 shows the theoretical values of transmission for various transmission media. These theoretical transmissions were calculated using the equation in Chapter 2 for transmission at material boundaries. The transmitted intensity for each boundary was calculated together to give the value transmitted after an initial sound intensity of 100, and so can be expressed as a percentage of intensity transmitted.

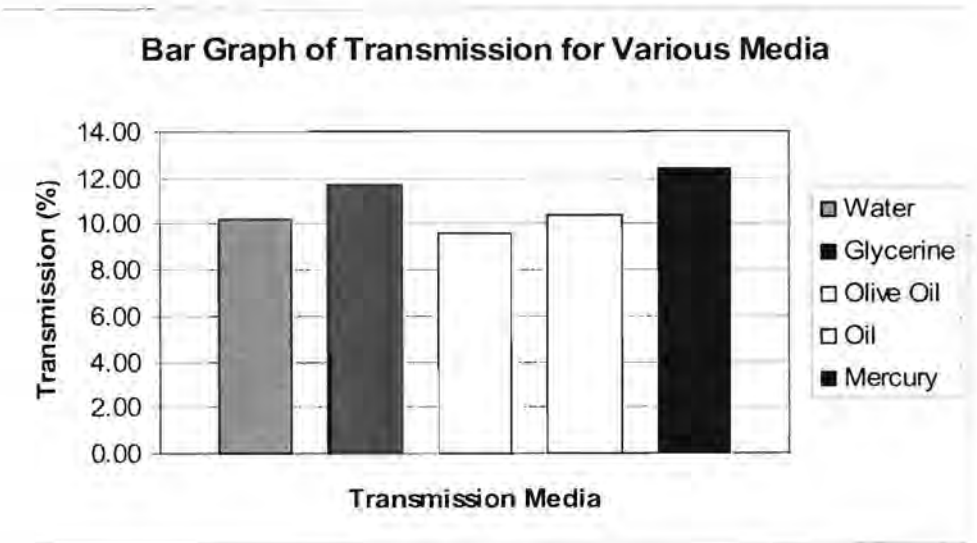

Graph 6-1 Theoretical Transmission through Various Media

6.1.2 Attenuation in the System

Looking at the tests done on the actual system, a number of interesting observations can be made. Graph 6-2 and Graph 6-3 show the sound intensity as a function of distance from the transducer. These values were taken with the use of a custom built PZT hydrophone. The intensities were expressed as a voltages as these graphs only serve as comparative and not absolute references. The Vibracel device was used again, with the amplitude set to 50% giving an average power of 70 Watts. The temperature was maintained at a constant 23°C by circulating water. The water level was maintained at 35mm above the transducer face for both receptor vessel and the coolant.

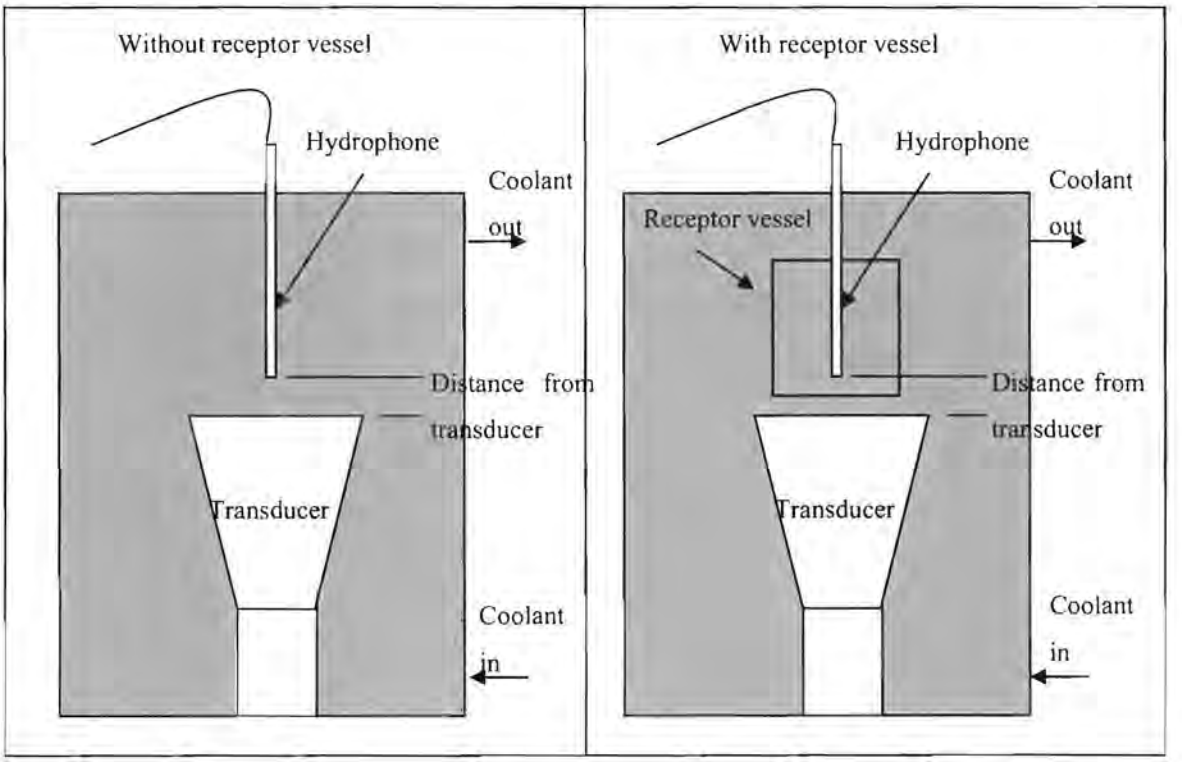

Figure 6-1 Apparatus used to Measure Attenuation over Distance

Two sets of readings were taken: one without the receptor vessel present, and the other with the receptor vessel present. The experimental set-up is shown in Figure 6-1. Graph 6-2 shows the sound intensity as a decaying exponential with a sinusoid superimposed on top of it. This demonstrates very well the exponential decay of a sound wave in a lossy medium, as well as the standing waves that are set-up in the

water because of the reflection boundaries at the water surface (i.e. water – air boundary reflecting 99% of the sound energy – based on Equation 2-9).

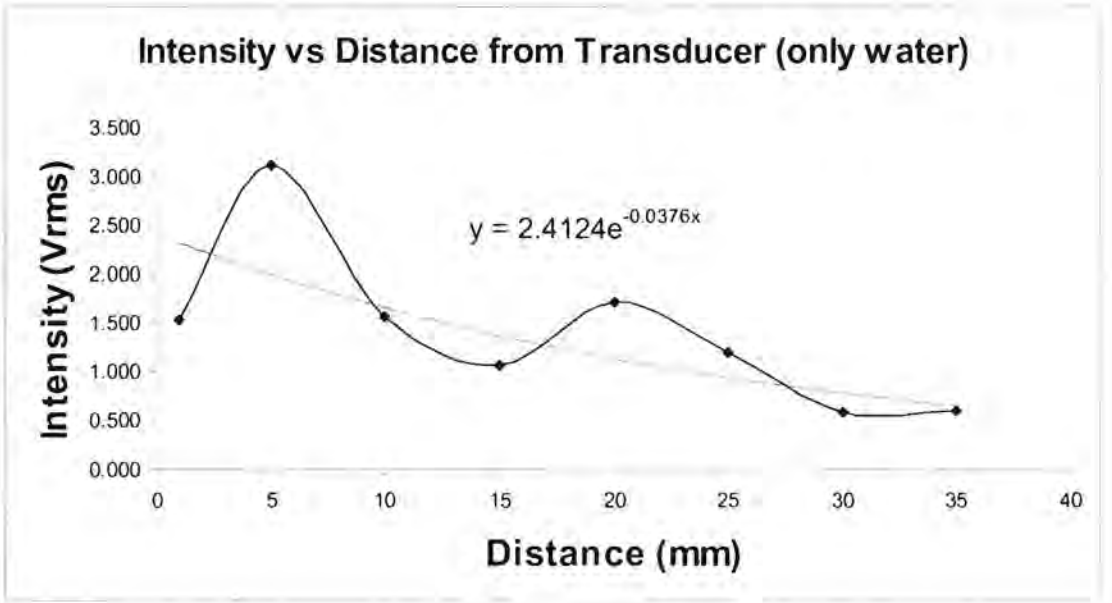

Graph 6-2 Sound Intensity as a Function of Distance in Water, showing Standing Wave Pattern and Exponential Falloff due to Absorption.

Graph 6-3 below shows the intensity measured under identical conditions, except that the bottom of the plastic vessel was placed in between the transducer and the hydrophone showing the effect on the plastic vessel, in terms of the combined effect of absorption in the plastic and sound reflection at the material boundaries. It shows an absorption coefficient 43% larger compared to the above tests with no receptacle. This is quite substantial, and one of main reasons for the investigation into the transmission media was to attempt to reduce this absorption.

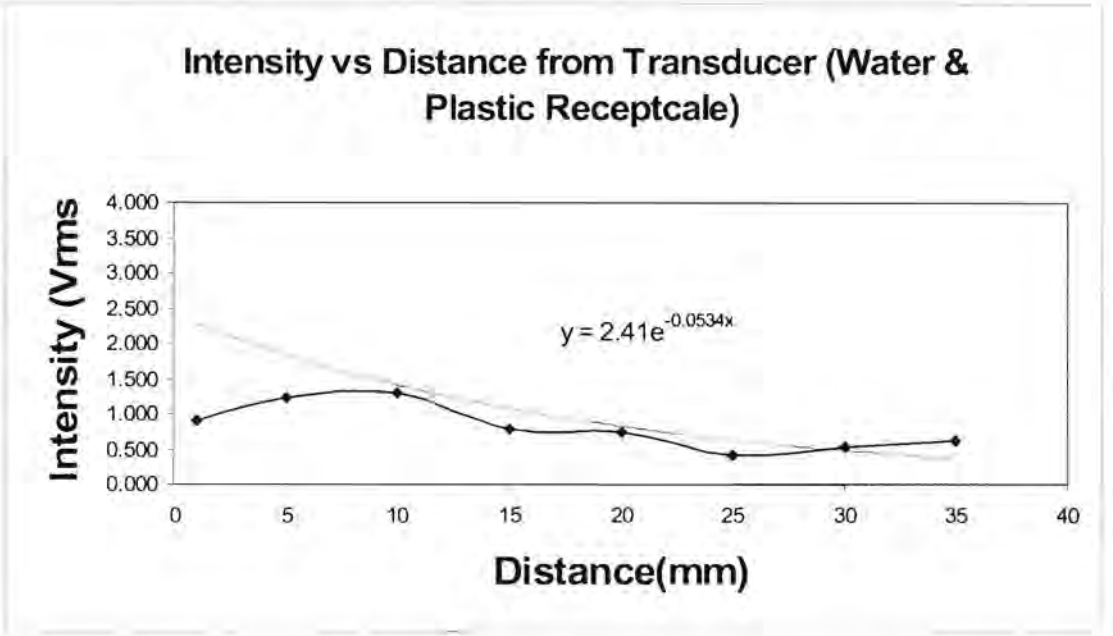

Graph 6-3 Sound Intensity as a Function of Distance in Receptacle, As above but showing a Smaller Intensity.

6.1.3 Affect of solutes on Vapour Pressure

In order to fully understand the results presented in the next section, a review of Raoult's Law follows:

> *The vapour pressure increase of the solvent, ΔP, of a solution equals the vapour pressure of the pure solvent, P_0, times the mole fraction of solute, X, in the solvent.[11] Pg 497*
>
> *I.e.* $\Delta P = P_0 X$

This implies that the addition of a solute or salt to the transmission medium has the effect of increasing the vapour pressure and, consequently, the threshold pressure, causing a suppression of cavitation amongst other things.

6.2 Transmission Media

The transmission media that were expected to work well, based on reflection calculations, were those with acoustic impedances of between 1.7 and 27.3 MRayls, having a low viscosity and high vapour pressures. However, a wide cross-section of liquids were chosen for testing to confirm the above assumptions.

6.2.1 Testing of Various Media

The tests carried out on the media used the standard set-up described in Chapter 3 with a few modifications. The first being that the medium could not be circulated, as there was not sufficient quantities to do so. This meant that the same liquid was used for successive tests, making cooling it necessary. This was achieved by inserting a copper pipe coil through which cooling water was passed, acting as a heat transfer mechanism, cooling the medium down to 23°C before each test. The amplitude setting put at 100% gave a power of about 160 Watts. The gap between the transducer emitting-face and the receptacle was 1mm and the transition medium and water in the receptacle was at a level of 35mm above the transducer emitting-face. Once again the foil sample was placed in the receptor vessel with a vertical orientation.

Graph 6-4 below shows the disruptive index for the media tested. Water was the medium used in all previous tests, implying that we needed a medium that produced higher disruptive indices in order to increase the transmission. (These results were the average of three foil tests).

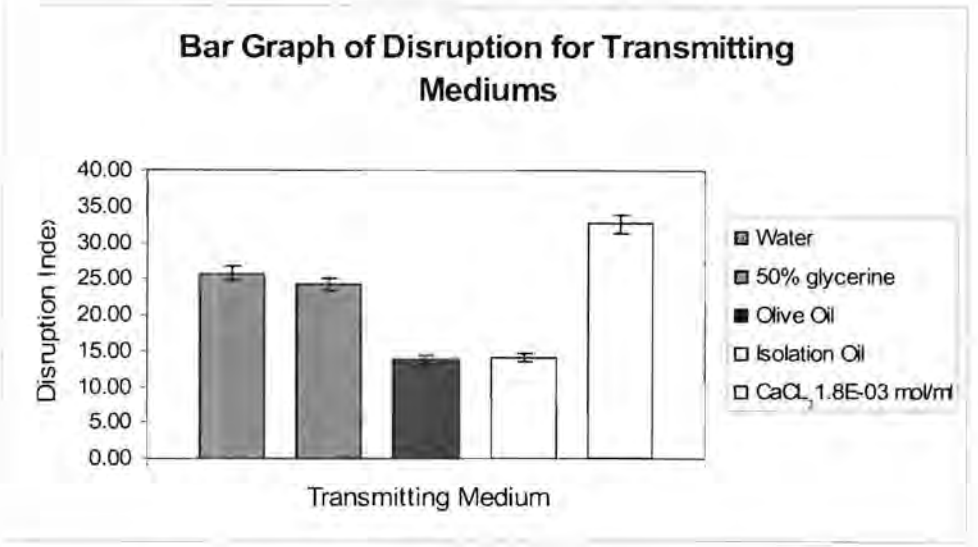

Graph 6-4 Bar Graph of Transmitting Media (at 23°C)

Once again, in Graph 6-4, it can be seen that both the oils performed very badly even though they suppressed the cavitation, as visually confirmed. It was evident that the viscosity caused large absorption of sound energy. The medium labelled "50% Glycerine" consisted of a 50% water, 50% glycerine mixture and produced a slightly worse disruption index than water due to the presence of cavitation (as much as in pure water), and the high viscosity media apparently absorbing more energy than lower viscosity media. The one medium that increased the transmission, with a disruption index of 27% higher than water, was the $CaCl_2$ solution. This was most likely because the vapour pressure was increased according to Raoults' Law, as the cavitation could visually be seen to have reduced significantly. However, the concentration of 1.8×10^{-03} mol/ml was randomly chosen and needed optimisation.

6.2.2 Optimising $CaCl_2$ Solution Concentration

Using the same experimental set-up as above, a set of foil tests were conducted with varying molar concentration of $CaCl_2$ in water.

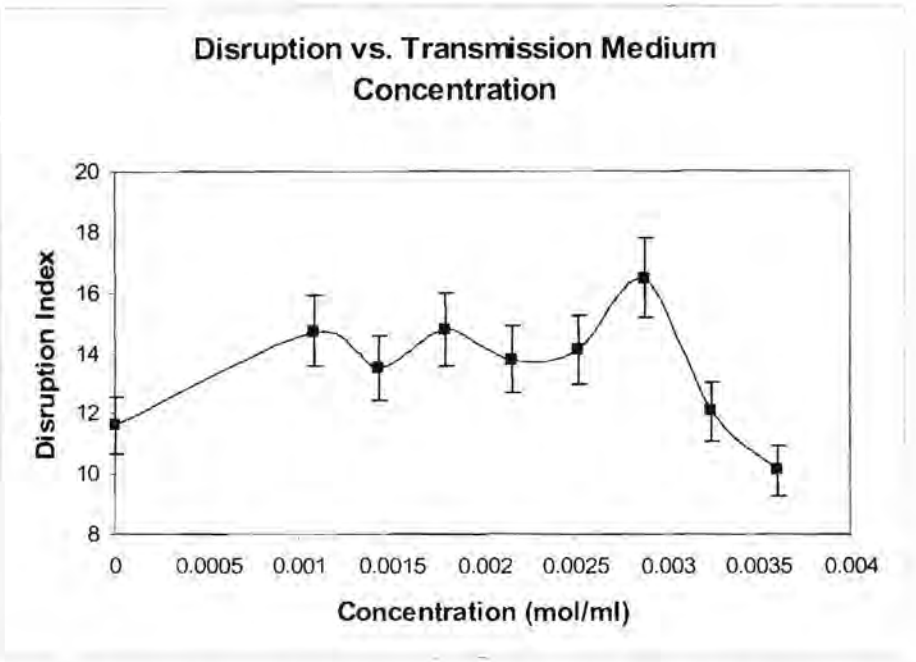

Graph 6-5 Concentration Optimisation (at 23°C), showing the Optimum Molar Concentration in terms of Transmission.

Graph 6-5 shows a band between 0.001 and 0.003 mol/ml with an average disruptive index of 22% larger than that of plain water. This region has a few other maximums but these are probably extremes caused by random errors. It was nonetheless obvious that the transmission falls off rapidly for concentrations above 0.003 mol/ml. This is possibly an increased viscosity causing the medium to absorb energy, thereby reducing the transmission.

7 Streaming

As mentioned before, the effects of acoustic streaming provide a mixing and stirring action. It was desirable to maximise these mixing effects to improve the dispersion process and therefore it was critical that the factors influencing streaming are discussed and quantified in the context of a disruption cell. This chapter looks at the streaming patterns set up in the treatment vessel and how these are affected by factors such as amplitude (or acoustic intensity), the water gap between the transducer and the vessel, the vessel size, and, finally, the volume of liquid in the vessel.

7.1 Test Conditions

The tests conducted in this chapter were done under the conditions that produced the best disruption as set out in previous chapters, namely a 50ml plastic bottle 1mm above the transducer, and water both inside and outside the receptacle. The height of the coolant/transmission medium was set at 35mm above the transducer face. Only the variable under investigation was changed to see its effect on acoustic streaming. The streaming patterns of the tests that were done used the same basic apparatus shown in Figure 7-1.

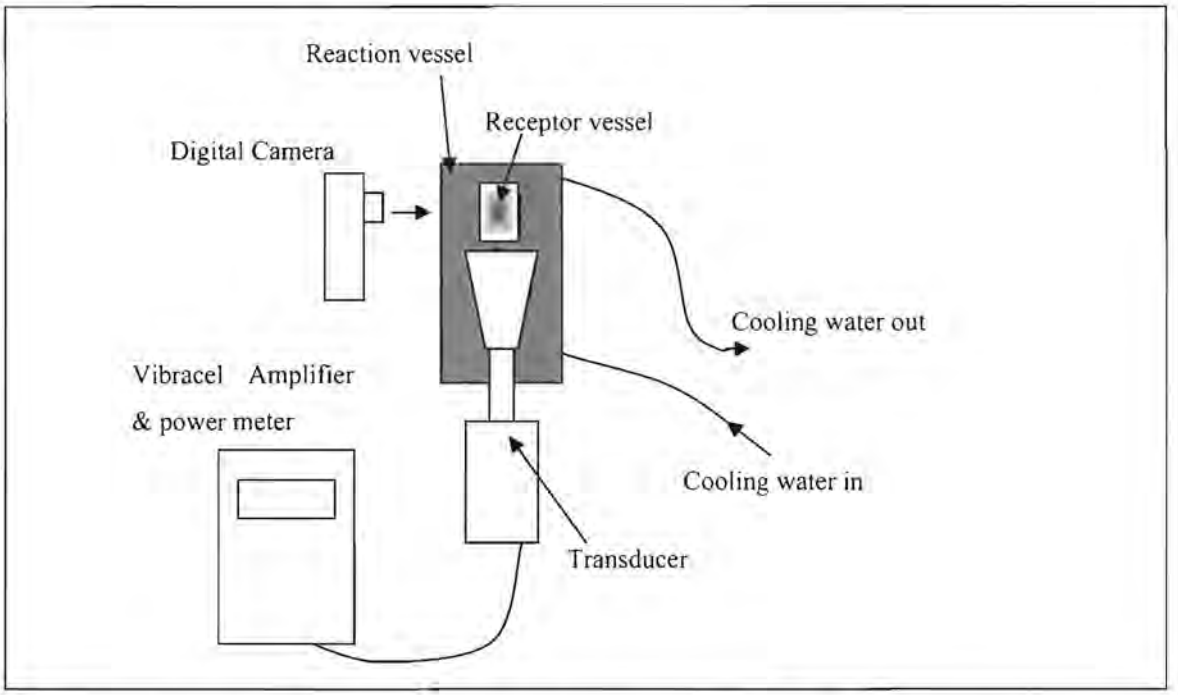

Figure 7-1 Streaming Measurement Apparatus, showing the Physical Arrangement of the Apparatus.

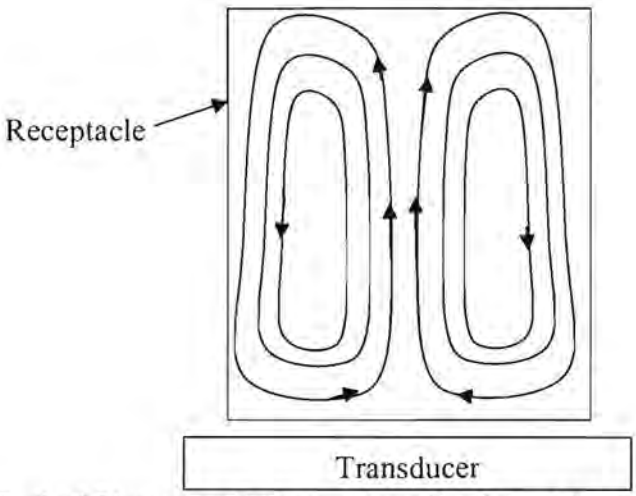

Figure 7-2 Typical Streaming Pattern, where the Curved Lines and Arrows Represent the Path and Direction of the Streaming Water.

In Figure 7-2 the position of the transducer is shown, where the rectangle labelled "receptacle" above the transducer represents a cross section of the cylindrical receptor vessel with a typical streaming pattern. These streaming patterns were particularly suited to dispersion of solids due to the fact that the solvent flows to the centre of the

bottle. This moved solids to the regions of high intensity ultrasound (the centre of the vessel). Only once the solid was damaged or lightened sufficiently would it be lifted and removed by the streaming forces.

The streaming was predominantly symmetrical around a vertical line in the centre of the vessel. As mentioned in Chapter 3, the patterns were analysed with the aid of aluminium powder in water and a digital video camera. Using a personal computer to step through the video frame-by-frame, it was possible to obtain the velocity of the streaming with reasonable accuracy and visually quantify the extent of the streaming.

Figure 7-3 Frame 18, shows the Aluminium being Picked up by the Streaming.

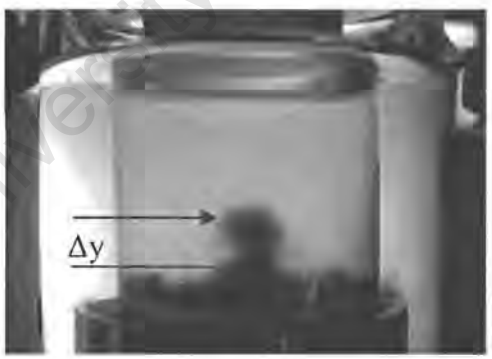

Figure 7-4 Frame 22, shows the Distance the Particles of Aluminium have Travelled between the Two Frames.

In Figure 7-3 Frame 18 and Figure 7-4 Frame 22 it can be seen how the velocity measurements were taken: divide Δy by the time between Frame 18 and 22 based on the fixed frame rate of 14.5 frames per second.

7.2 Acoustic Intensity

Graph 7-1 was obtained using the above method to measure the velocity of the streaming and varying the amplitude of the transducer. This displays an apparent linear relationship between velocity and amplitude. Amplitude is also related to intensity in this context due to the transducer load being consistent. These results are confirmed by the Equation 2-6 $v_0 = \frac{I_0 R^2 \omega^2}{3\rho_0 c_0^4}$ where the streaming velocity (v_0) is linearly proportional to sound intensity (I_0). Based on the results, it can be confirmed that the increase of acoustic intensity causes an increase in streaming velocity for this particular arrangement.

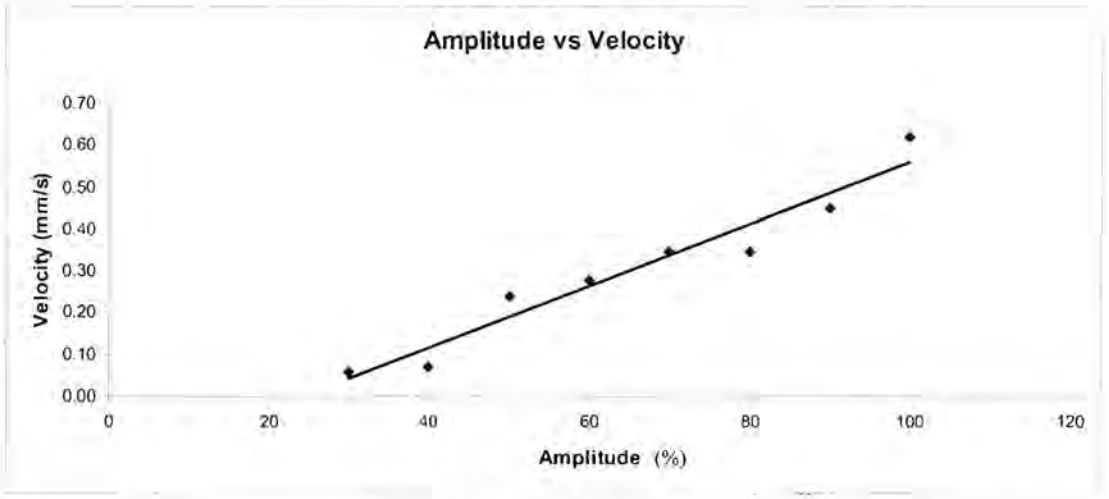

Graph 7-1 Streaming Velocity as a Function of Amplitude, where the Streaming Velocity seems to Increase Linearly with Amplitude.

The 'Glass vessel' trace in Graph 4-1 shows the relationship between amplitude and power for the Vibracel unit, which can be used to calculate the power values in the above Graph 7-1.

7.3 Distance from Transducer

Looking at the results obtained from varying the gap between the receptacle and the transducer in Graph 7-2, yet another interesting phenomenon related to acoustic intensity can be seen. Graph 7-2 shows the velocity decaying exponentially as the gap was increased. This was not a direct streaming effect but rather confirmation that the water gap between the vessel and transducer absorbs the sound energy exponentially as a function of distance (Equation 2-12). This again confirms and correlates with the test results for destruction of the foil samples. Graph 7-2 shows that the larger the acoustic intensity (or the closer the receptacle vessel to the transducer), the more pronounced the streaming effects.

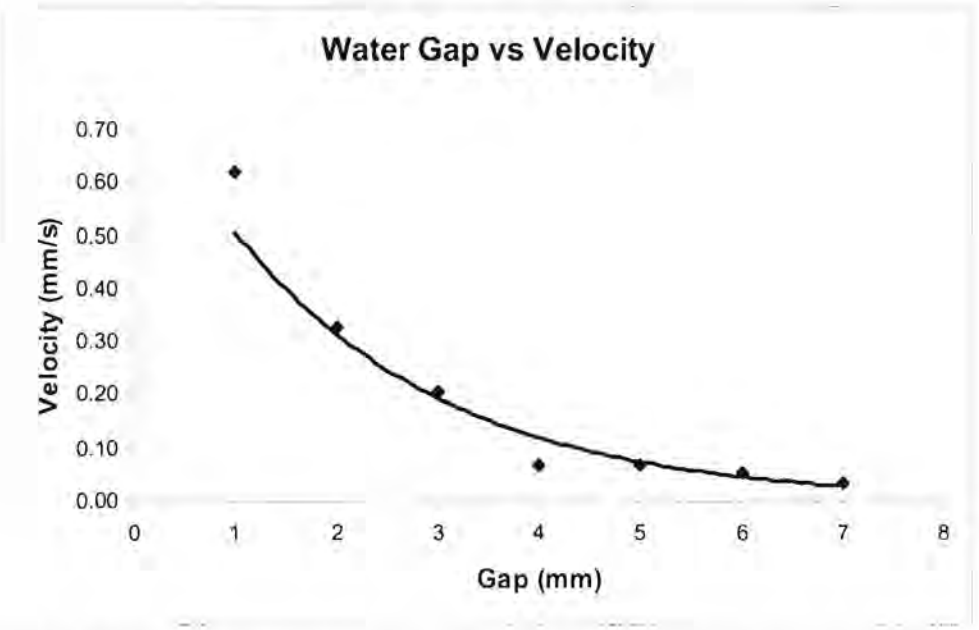

Graph 7-2 Streaming Velocity as a function of Transducer – Receptacle Distance, Showing a more Violent Streaming action for Small Transducer Receptacle Gaps.

7.4 Bottle Size

The reduction of the bottle size from 50ml to 20ml and 10ml respectively had an interesting effect where the aluminium powder was lifted off the bottom of the vessel, but only held up and not circulated. This implies the smaller vessels have a more or less constant radiation pressure across the base, producing images such as that in Figure 7-5, as opposed to radiation pressure that is more pronounced in the centre allowing the liquid to circulate down the circumference and up in the middle (as in the 50ml vessel). This finding was consistent with experimental results in Beyer [8] where the magnitude of velocity was a function of the acoustic beam radius and the tube (bottle) radius. It shows the circulation velocity increasing with an increase in the ratio of beam radius over tube radius.

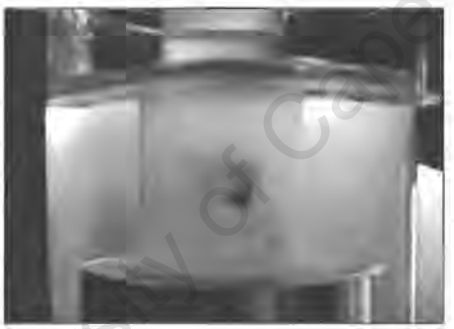

Figure 7-5 20ml Bottle Constant Radiation Pressure, where the Aluminium Powder was Held off the Bottom of the Receptacle and not Circulated as in Larger Vessels.

Increasing the bottle above, the 50ml to 100ml vessel had very little effect on the streaming pattern, only reducing the extent of the streaming as would be expected from a larger volume having higher inertia.

7.5 Volume Levels

As was expected, the variation of water level in the vessel had very little effect in terms of the extent of the streaming as a function of the total volume. However, it was noticed that the streaming velocity increased slightly with an increase of volume. It was also noticed that the volume level of 10ml in the 50ml container deviated from the typical streaming pattern set out in the beginning of this chapter by being visibly more chaotic in nature. The apparent radiation pressure (based on the initial velocity) at the bottom of the vessel seemed to increase with an increase of volume, possibly because the loading of the system caused the acoustic intensity at the vessel base to increase. This effect cannot be used successfully however, as an increase of volume would dilute the streaming and, more importantly, reduce the cavitation density which would be undesirable.

7.6 Conclusion

Based on the tests conducted, it was clear that streaming, or more precisely radiation pressure, was proportional to acoustic intensity, thus agreeing with the theory [4]. The presence of a volume large enough to enable circulation was important.

8 Thermal Shocking

This chapter was concerned with the use of thermal cycling to increase the dissolving qualities of the solvent as well as increasing the disruptive force of the cavitation. It first looks at the dependence of violent cavitation on temperature. Next, the effect of introducing solvents at different temperatures, and finally the real temperature profile calculations, using thermal modelling of the system.

8.1 Test Conditions

A fluid dispenser (on loan from industry) provided a flexible and accurate means of adding the solvent in the correct volumes, at a set temperature and at the right time intervals. The fluid dispenser consisted of two pump, storage and delivery systems: one for the hot solvent and one for the cold solvent. The unit's delivery system and experimental environment is shown in Figure 8-1 and Figure 8-2.

Figure 8-1 Picture of Fluid Dispenser Configuration, showing the receptacle with the dispenser delivery pipe just inside it and the glass cup-horn containing the transmitting fluid (in this case water).

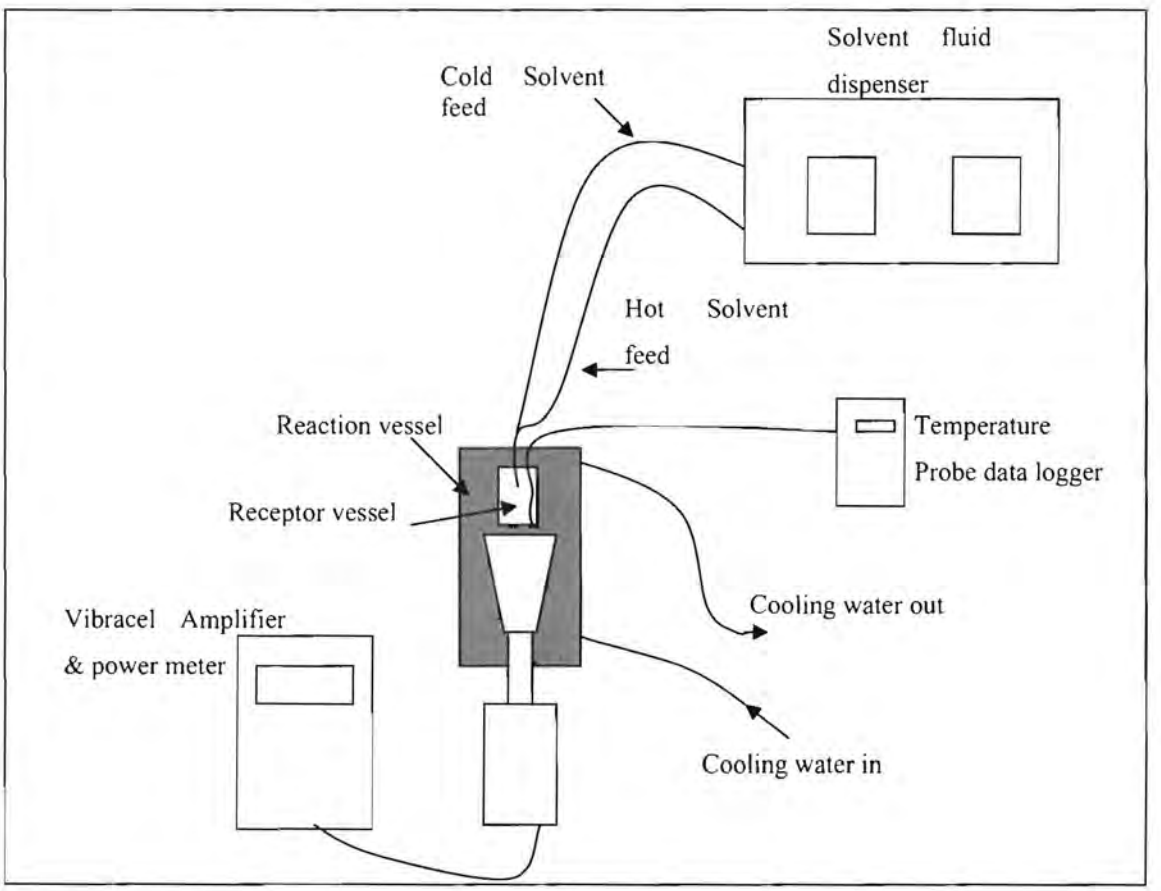

Figure 8-2 Thermal Shocking Apparatus, showing the Layout of the Apparatus

8.2 Effects of Temperature on Cavitation

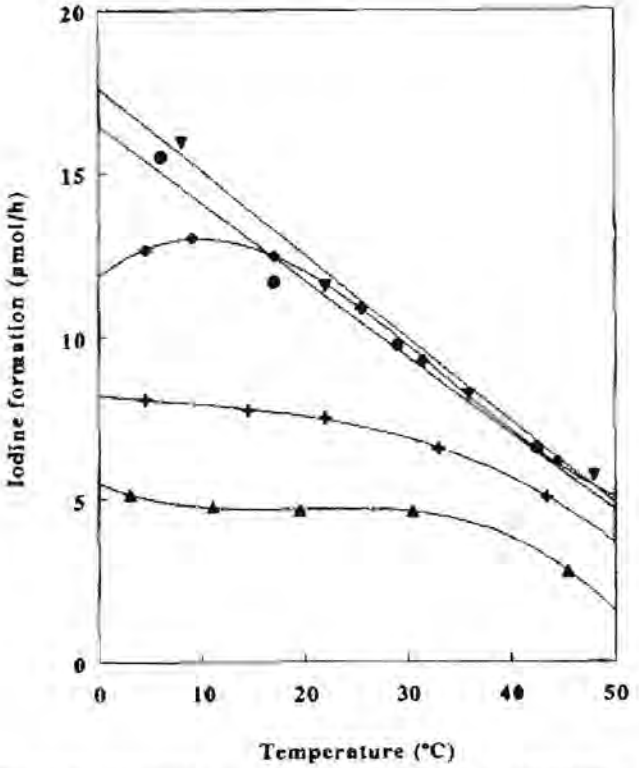

Figure 1 Variation with temperature of the rate of sonochemical oxidation of iodide using 20 kHz irradiation with an X-large tip. (▲) 21 W; (+) 32 W; (◆) 42 W; (●) 56 W; (▼) 72 W. Each point

Graph 8-1 Iodine oxidation as a result of cavitation as a function of Temperature [19], showing fall-off in oxidation with and increase of temperature.

Graph 8-1 from Entezari and Kruus, shows the cavitation in terms of iodine oxidation as a function of temperature for a system using ultrasound at 20 KHz . It clearly shows a decrease in cavitation for an increase in temperature, and for this reason the temperature needs to be controlled quite accurately. (These values are not necessarily the case with water but show the importance of thermal control.) It must also be noted that samples may be sensitive to high temperatures and an easy method of calculating/measuring the real temperature is required. [19]

Increasing the temperature of the solvent increases the dissolving of the organic solid. The benefits of a high temperature solvent are obvious and therefore the temperature

needs to be allowed to rise as high as possible, but without reducing the cavitation too much. For these reasons it was essential to understand the thermal system.

8.3 Use of Analogue Computers in Temperature Calculations

Analogue computers were used to accurately predict the real temperatures of the solvent base on the measured temperatures, as well as predicting temperatures of untested situations. These analogue computers were electrical in origin yet provide a fast, flexible method of solving differential equations. The thermal system can be modelled in electrical terms using the equivalent parameters set out in Chapter 2. This enables the real temperature sensor to be modelled and actual dynamic temperature profiles can be calculated.

8.4 Temperature Profiles

Temperature profiles were measured with an LM35T electronic temperature probe that was inside the treatment vessel. The treatment vessel (50ml polyprop.) was then placed in the Vibracel 68mm cup horn along with the transmitting fluid (water at 23°C) providing cooling as well as acoustic transmission. The cooling fluid was circulated to ensure that the temperature of 23°C was maintained. (Flow rate for this was 250ml/min). Graph 8-2 shows a typical temperature profile record, where the effects of adding the hot and cold water can each be clearly seen.

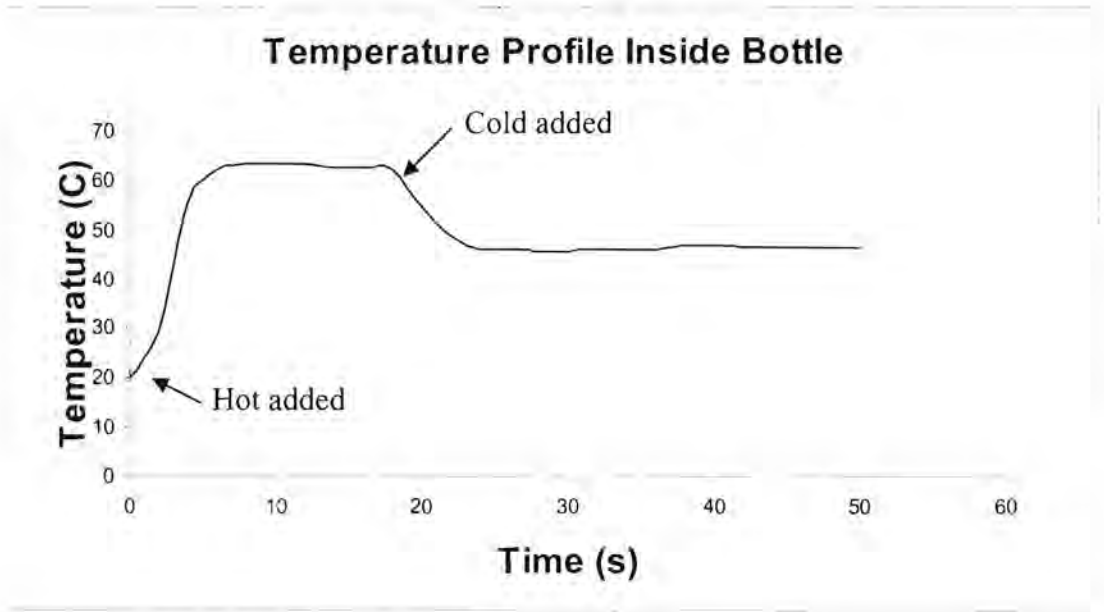

Graph 8-2 Typical Temperature Profile, showing the Change in Temperature over Time as the Hot Water was Added and then the Cold.

8.4.1 Varying Volume Ratios

To fully understand the effect of different volumes and temperatures of the solvent being added to the container, a set of tests were carried out and the temperature profiles were recorded. Using the apparatus as described and shown in Figure 8-1, Graph 8-3 shows the effect of varying the ratio of hot (90°C) and cold (23°C) water while keeping the final volume at 30ml.

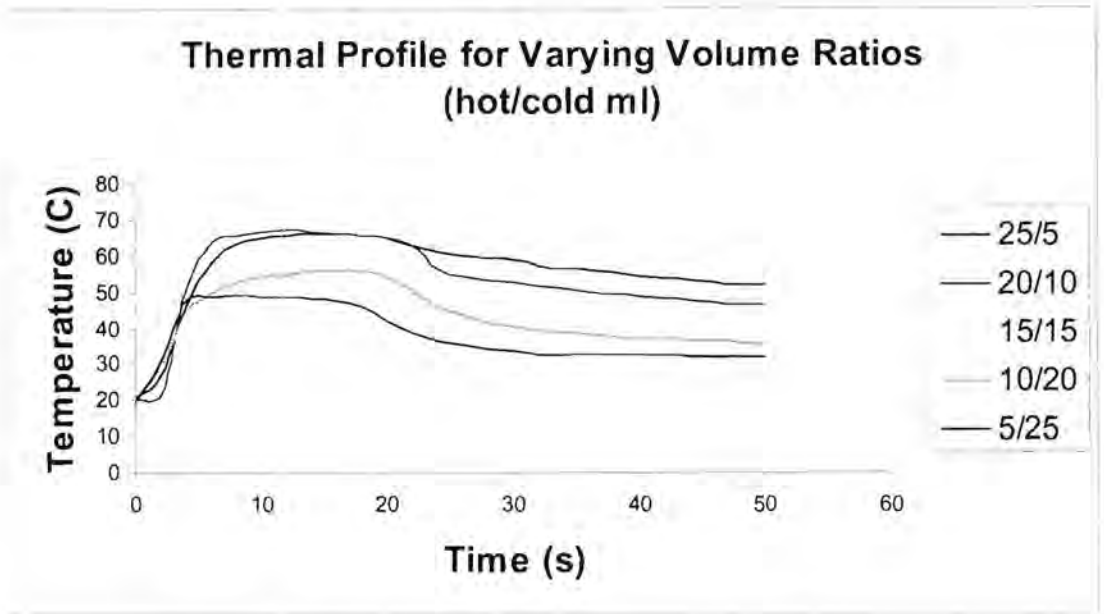

Graph 8-3 Thermal Profiles for Varying Ratios, where the 25/5.. etc. Represents the Volume of Hot Water / the Volume of Cold Water.

To get the profile above, the hot water (the solvent in this case) was introduced first and, after a delay of 15 seconds, the cold water was added. Graph 8-3 gives a fair indication of the temperatures involved and shows that the temperature apparently doesn't go above 70°C. As was presumed, the larger the amount of hot water introduced, the higher the temperature throughout the profile, and, subsequently, the final temperature (after 50 seconds) was higher.

8.4.2 Equivalent Circuits

Based on the above tests with variable volume ratios, the effectiveness of equivalent circuits in calculating the temperature profiles can be seen. Figure 8-3 below shows an equivalent circuit (analogue computer) that was used to calculate the profiles. The various subsections of the circuit can be seen, along with their thermal equivalents.

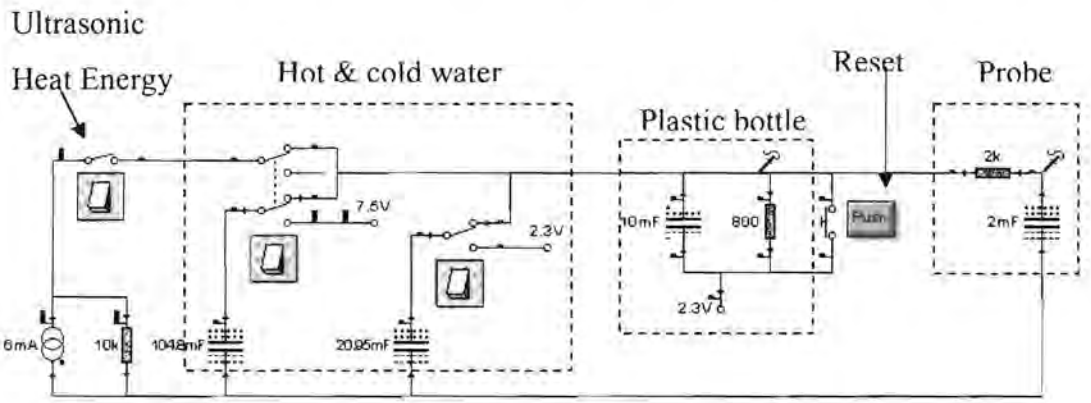

Figure 8-3 Thermal System Equivalent Circuit

The hot and cold water are represented as capacitors (heat storage) charged to a specific voltage (temperature), using switches to introduce the capacitance (water volume) to the system at the correct time. The plastic bottle was represented as a capacitor (heat capacity) and a resistor (thermal conduction) to a voltage source (the cooling liquid), and the temperature probe, as mentioned already, was modelled as a low pass filter. The ultrasonic energy (heating) is represented as a current source. The two probes, one in the plastic bottle box and the other in the temperature probe box, were used to produce real time traces of the real and the measured or apparent temperature.

Graph 8-4 displays these traces where the components were tuned to simulate the 5ml hot and 25ml cold settings. It was interesting to note that the real temperature was quite different in shape and magnitude to the measured value. This discrepancy in the profiles was due to the time lag or slow response of the temperature sensor in registering the measured temperature.

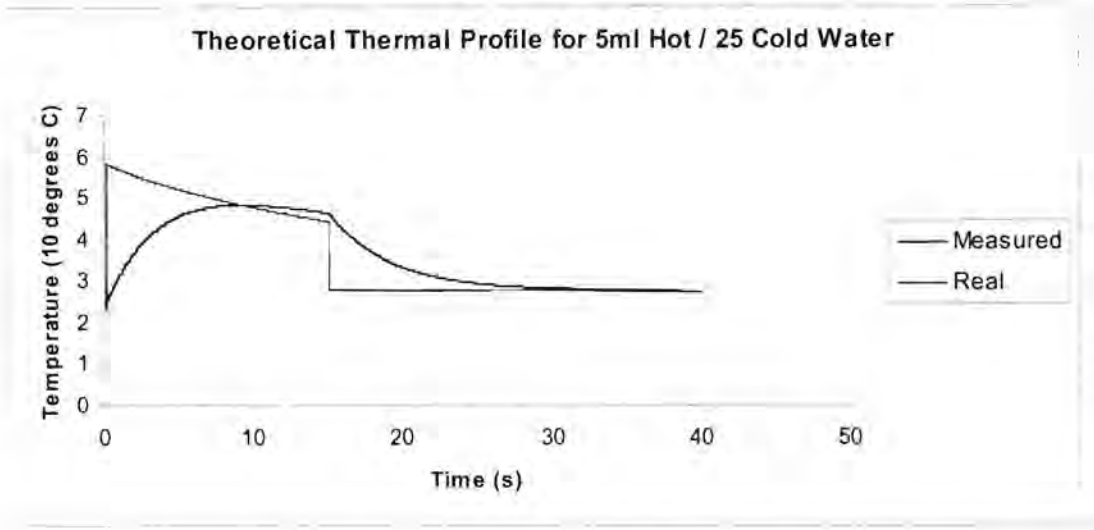

Graph 8-4 Theoretical Thermal Profile for 5ml hot / 25 ml cold.

This shows the temperature at which the liquid in the receptacle was initially at, just after t=0 seconds, and the discrepancy between the measured and real values. Anyone wanting to use this thermal shocking needs to realise that for all the simulations done, the maximum real temperature was about 20% higher than the maximum measured temperature owing to the time constant of the temperature sensor. This is important in terms of raising the temperature above a value that would suppress cavitation and/or damage the sample in some undesirable way.

8.4.3 Ultrasonic Energy Effects

Tests done up to this point have been with the transducer switched off so as to simplify the analysis until the system was well understood. The effect of switching on the transducer can be seen below in Graph 8-5 where the ultrasound introduces heating energy into the system, thereby raising the thermal profile. This can be simulated by modelling the heat energy as a current source.

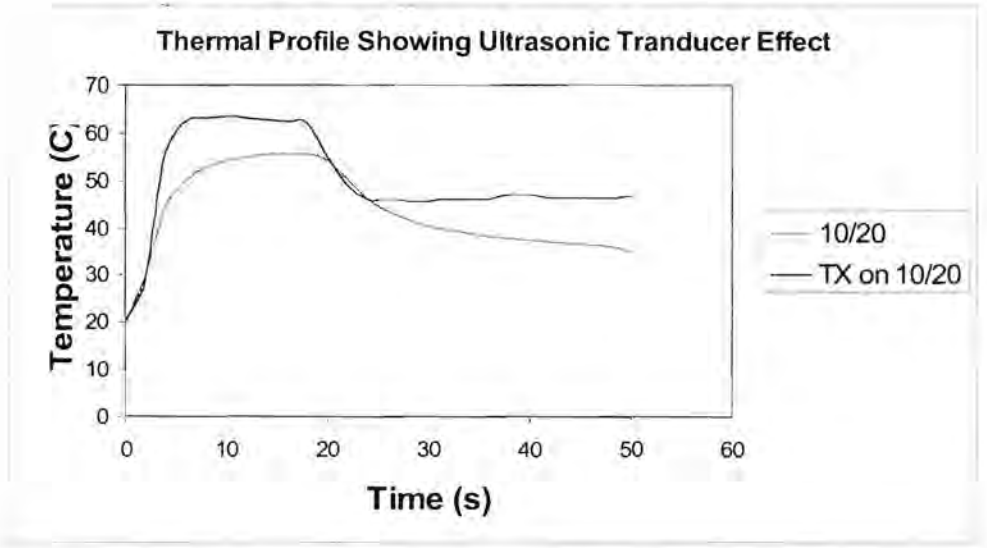

Graph 8-5 Effect of Introducing Ultrasonic Energy, where the Introduction of Ultrasonic Energy causes a Noticeable Increase on Temperature

It must be noted that for the profiles shown above the transducer has the effect of increasing the temperature by 10°C. This must be taken into account and compensated for. Graph 8-6 shows the temperature profile generated using the analogue computer simulating the transducer being switched on. The maximum temperature can be seen to be the same for real and measured case; however, it shows the difference in time duration at that maximum temperature. This effect still needs to be considered by the end user as the time at the maximum temperature is roughly 50 % longer than that implied by the measured profile.

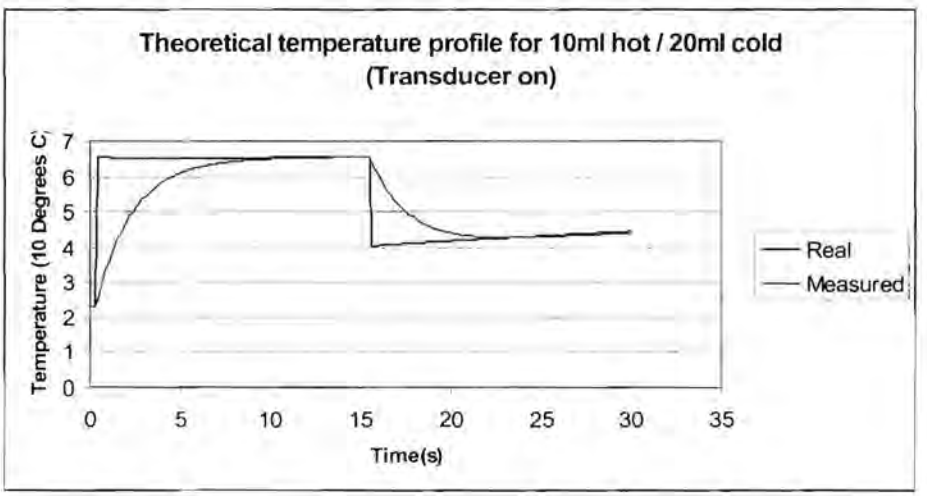

Graph 8-6 Theoretical Temperature Profile (Transducer Switched on)

9 Conclusion & Future Recommendations

The factors influencing cavitation, streaming and ultimately dispersion were investigated and optimized to produce a number of useful methods or apparatus, as outlined below.

The use of a digital image processor for the analysis of foil samples to give both numerical area values for damaged and destroyed foil, and to show spatial distribution of the cavitation field, proved to be invaluable. It made possible large numbers of tests due to its speed and need for little user intervention, while still maintaining consistency and accuracy throughout the testing.

The problem of acoustic saturation at high powers was overcome in a number of ways. Firstly, the static pressure or the differential pressure method provided an increase in destruction (cavitation damage) of 250 ± 20% in the Vibracel unit and 139 ± 11% in the tri-reactor bath. The reason for the tri-reactor having a lesser increase in destruction with the differential pressure method was because the saturation effect was already partially overcome by the use of multiple transducers. The use of three transducers, and hence three paths for the acoustic energy to travel through, provided an increase of destruction by 240 ± 19.2% compared to the same apparatus with only one transducer active but at the same power as the three transducers. The combined effect of differential pressure and the use of three transducers provided an increase of 330 ± 26% in destruction. The third method of reducing saturation was the use of a salt solution, to raise the cavitation threshold by limiting cavitation that absorbs energy in the transmission medium. This only increased the destruction by 122 ± 9% but could be used in conjunction with the above pressure differential methods.

The investigation into streaming provided important information on acoustic streaming in the context of a small vessel. The tri-reactor unfortunately didn't produce

any notable streaming effect, making it a very poor option due to the lack of macro-mixing. However, future work may look into making an unbalanced multiple transducer bath. It might also be an option to sometimes drive only one transducer on the tri-reactor vessel, to unbalance the acoustic field. It must be noted that for the cup horn set-up, the streaming was proportional to sound intensity and that the vessel needs to be over 30ml in volume to allow significant streaming.

Thermal shocking provided additional dispersion capability by increasing the cavitation strength, as well as increasing the ability of the solvent to dissolve. The use of equivalent circuits to estimate the real temperature profiles can be used to decide on the fluid dispenser settings, so as not to exceed the critical temperature of the specific organic compound.

In conclusion, the differential pressure, multiple transducers and salt solution provided an increase in acoustic intensity in the receptacle, which was the goal of the research. However, the combined effect of combining the salt solution with the pressure and multiple transducers is suggested for future work. Although the streaming was quantified for the existing system, more work could be done to increase the streaming amount and violence, particularly in the multiple transducer environment.

10 References

1. Sonochemistry, T J Mason, , 1990.
2. Sonics, Hueter & Bolt, John Wiley & Sons, Inc., 1955.
3. Ultrasonics, Dr. Ludwig Bergmann, G. Bell & Sons Ltd, 1938
4. Fundament Physics of Ultrasound, V.A. Shutilov, Gourdon & Breach Science Publishers, 1988.
5. Underwater Electroacoustic Transducers, D. Stansfield, Bath University Press, 1991.
6. Thermodynamics, Third edition, Cengel & Boles, McGraw Hill, 1998.
7. J P Perkins, Sonic Systems, application notes, 2002 (* Based on a paper presented at the Sonochemistry Symposium, Annual Chemical Congress, held at Warwick University, UK, 8-11 April 1986).
8. Nonlinear Acoustics, Robert T Beyer, Brown University lecture notes, 1974
9. University Physics ninth edition, Young & Freedman, Addison & Wesley Publishing, 1996.
10. Using Matlab™ to Analyse Foil Damaged by Ultrasonic Cavitation, C Foster, J Tapson, B Mortimer, 2002.
11. General Chemistry, Fourth Edition, Ebbing, Houghton Mifflin Company, 1991.
12. Ultrasonic Dispersion of Solid Drugs, Ricardo De Quieros, Cape Technicon, 2002.
13. Chaotic mixing generated by acoustic streaming, C. Suri, K. Takenaka, H. Yanagida, Y. Kojima, K. Koyama, Ultrasonics 40 (2002) 393–396.
14. Determination of velocity, size and concentration of ultrasonic cavitation bubbles by the phase-Doppler technique, N.A. Tsochatzidis, P. Guiraud, A.M. Wilhelm, H. Delmas, Chemical Engineering Science 56 (2001) 1831-1840

15. Measurements within cloud cavitation by means of X-ray attenuation device, G. Barouch, S. Legoupil, B. Stutz, R. Woo, Nuclear Instruments and Methods in Physics Research B, 2003.
16. Sonochemistry and sonoprocessing: the link, the trends and (probably) the future, Timothy J. Mason, Ultrasonics Sonochemistry 10 (2003) 175–179.
17. Polyethylene Joining Procedures, Plastic Pipe Institute, The Society of Plastic Industry, Inc. 1998.
18. A new ultrasonic method for fluid property measurement, S.O. Dymling, H. W. Person, T.G. Hertz, and K. Lindstrom, Ultrason. Med. Biol. Vol. 17, 497-500, 1991.
19. Effect of frequency on sonochemical reactions II. Tempertature and intensity effects, Mohammad H. Entezari and Peeter Kruus, Ultrasonics Sonochemistry Vol 3 (1996), Pg 19-24 ,1996.
20. http://pluto.apl.washington.edu/harlett2/artgwww/acoustic/medical/litho.html, 2002.

Appendix A

Image Processor Code Function

```
function r = foil(file,si)

Im = imread(file)                                   %Loading the Image
[m,n] = size(Im);                                   % getting size of image
figure, imshow(Im), title('original image');        % show image

% ----------------------------------------------    % damaged foil computation

Iadj = imadjust(Im, [], [0 1]);                     % normalize image

% figure, imshow(Iadj), title('scaled image');      % show image

Iedge = edge(Iadj, 'sobel', (2 * .11));             % edge detection

%figure, imshow(Iedge), title('binary gradient mask');   % show image

SE = ones(6,2);                                     % setting up dilate matrix

Iedgedil = dilate(Iedge, SE,'spatial',1);           % Dilating edges to group damaged foil

%figure, imshow(Iedgedil), title('dilated gradient mask');   % show image

seD = ones(3,1);                                    % setting up erode matrix
Ifinal = erode(Iedgedil,seD);                       % Eroding grouped areas to original size
Ifinal = erode(Ifinal,seD);
figure, imshow(Ifinal), title('Final damage image mask');   % show image

Dam = 100*(sum((sum(Ifinal)))')/(si);               % calculating percentage of
 black pixels to the total pixels

% ----------------------------------------------    % Destroyed foil computation

Ith = im2bw(Im,0.2);                % thresholding the image to reveal black destroyed areas

% figure, imshow(Ith), title('Threshold image');    % show image

seD = ones(3,1);
Itherode = erode(Ith,seD);                          % erodingto reduce outlier points

%figure, imshow(Itherode), title('eroded image');   % show image

Itherode = dilate(Itherode, SE,'spatial',1);        % Dilating to original size
figure, imshow(Itherode), title('Destroyed image mask');   % show image

Des = 100*((m*n)-(sum((sum(Itherode)))'))/(si);     % calculating percentage of black pixels to the
total pixels

r = [Des Dam];                      % returning Destroyed and damaged as a percentage
```

Appendix B

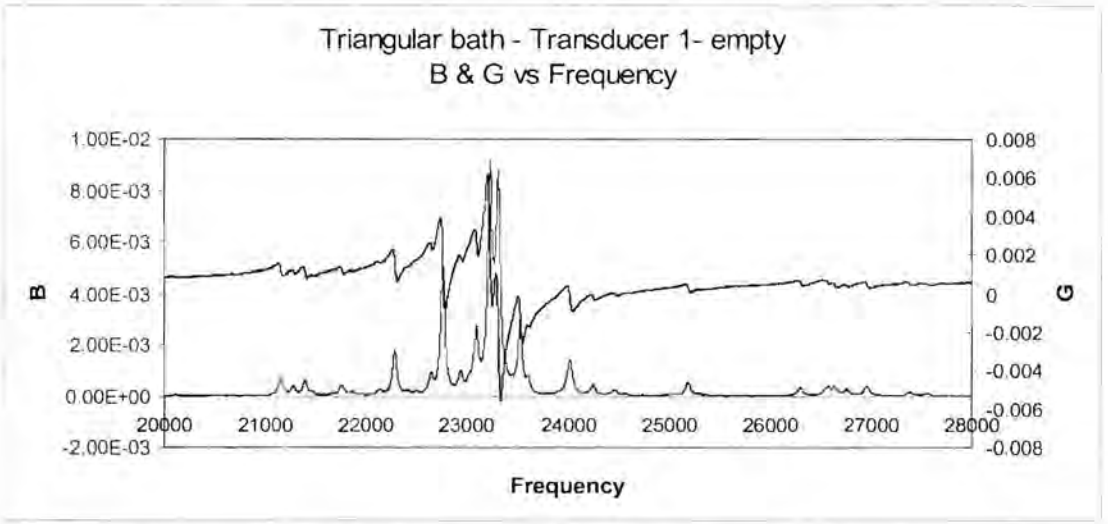
Triangular bath - Transducer 1- empty
B & G vs Frequency
B
G
Frequency
1.00E-02
8.00E-03
6.00E-03
4.00E-03
2.00E-03
0.00E+00
-2.00E-03
0.008
0.006
0.004
0.002
0
-0.002
-0.004
-0.006
-0.008
20000
21000
22000
23000
24000
25000
26000
27000
28000

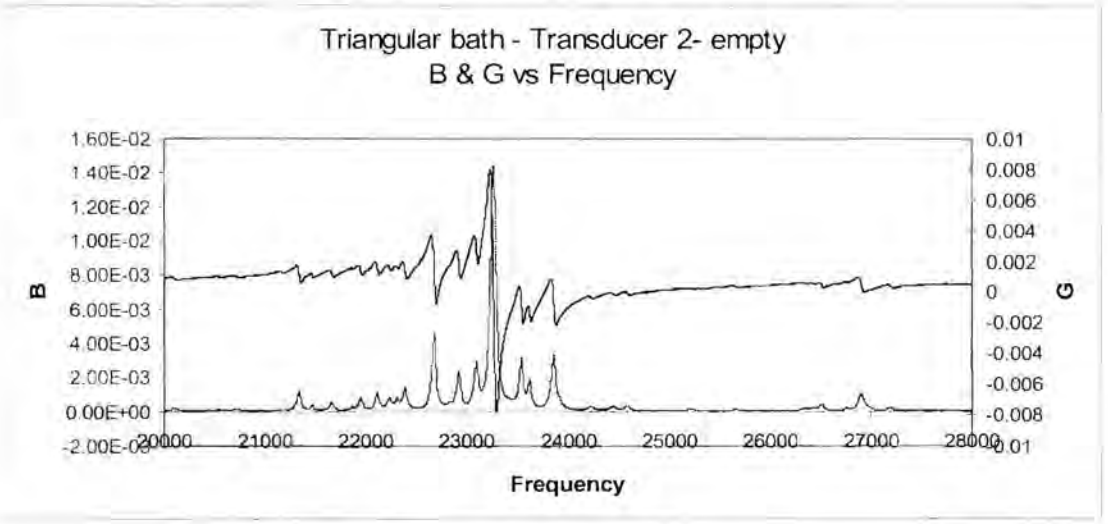
Triangular bath - Transducer 2- empty
B & G vs Frequency
B
G
Frequency
1.60E-02
1.40E-02
1.20E-02
1.00E-02
8.00E-03
6.00E-03
4.00E-03
2.00E-03
0.00E+00
-2.00E-03
0.01
0.008
0.006
0.004
0.002
0
-0.002
-0.004
-0.006
-0.008
-0.01
20000
21000
22000
23000
24000
25000
26000
27000
28000

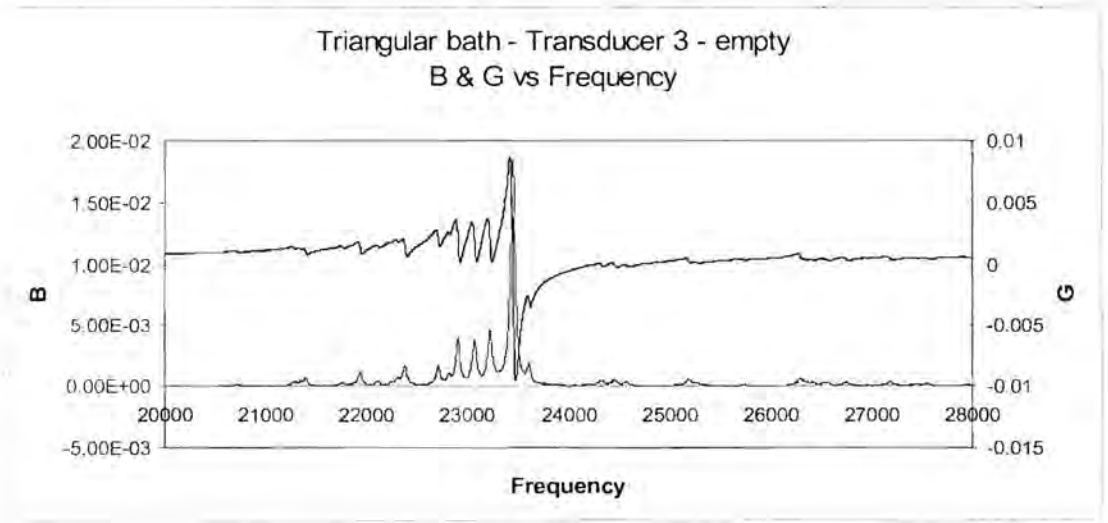
Triangular bath - Transducer 3 - empty
B & G vs Frequency
B
G
Frequency
2.00E-02
1.50E-02
1.00E-02
5.00E-03
0.00E+00
-5.00E-03
0.01
0.005
0
-0.005
-0.01
-0.015
20000
21000
22000
23000
24000
25000
26000
27000
28000

Appendix C

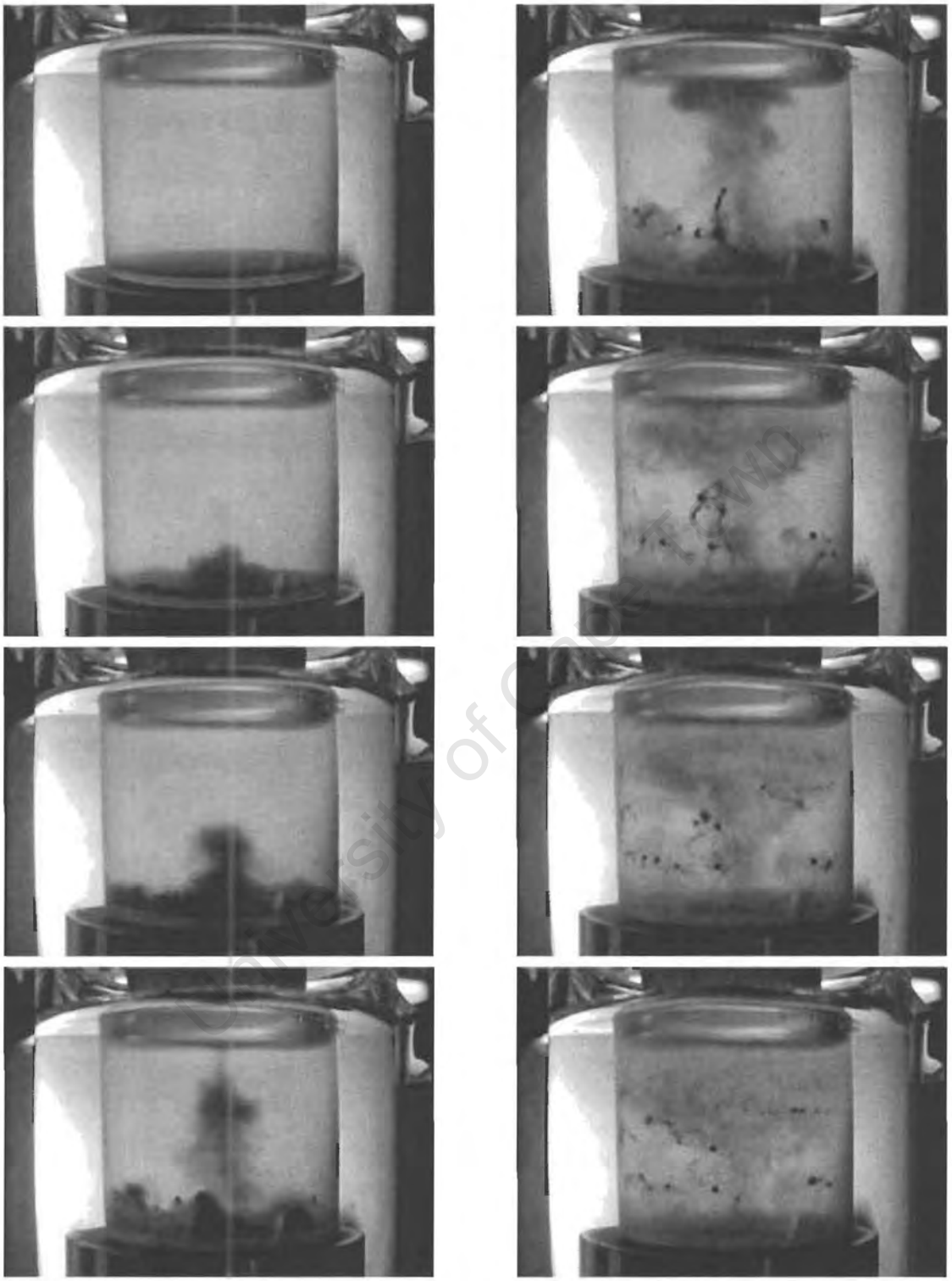

Appendix D

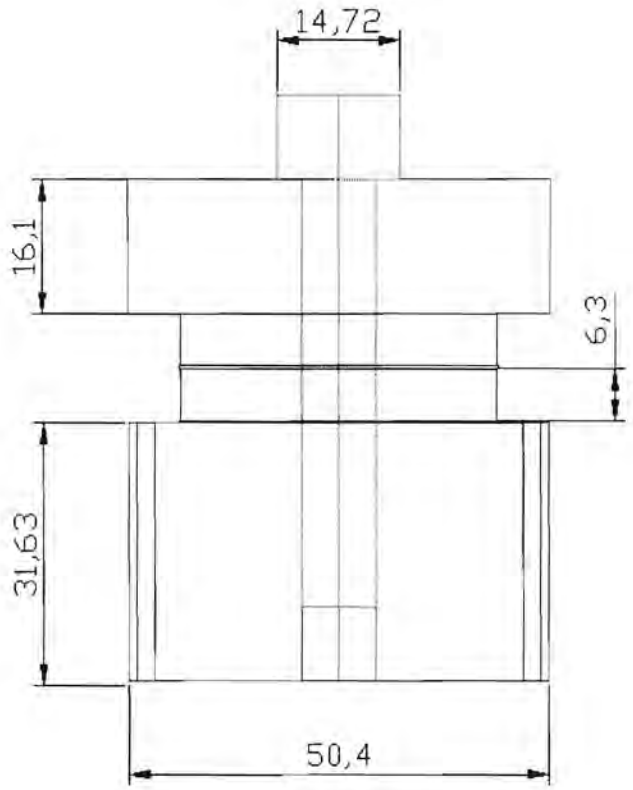

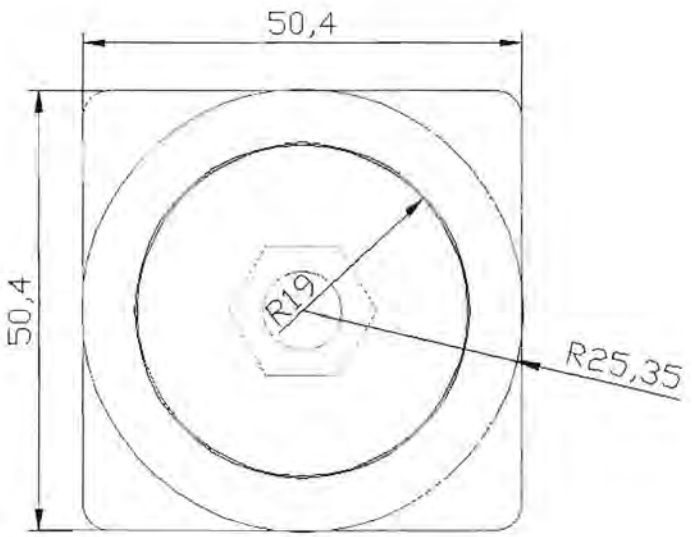

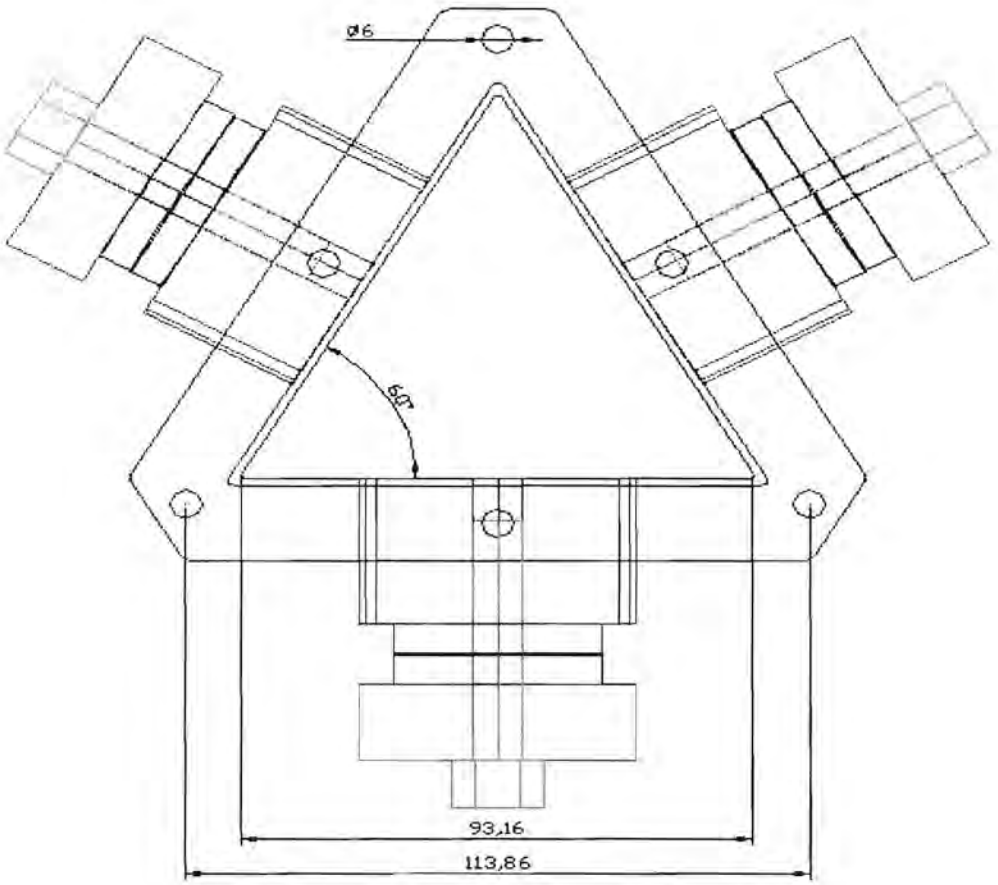
ø6
60°
93,16
113,86

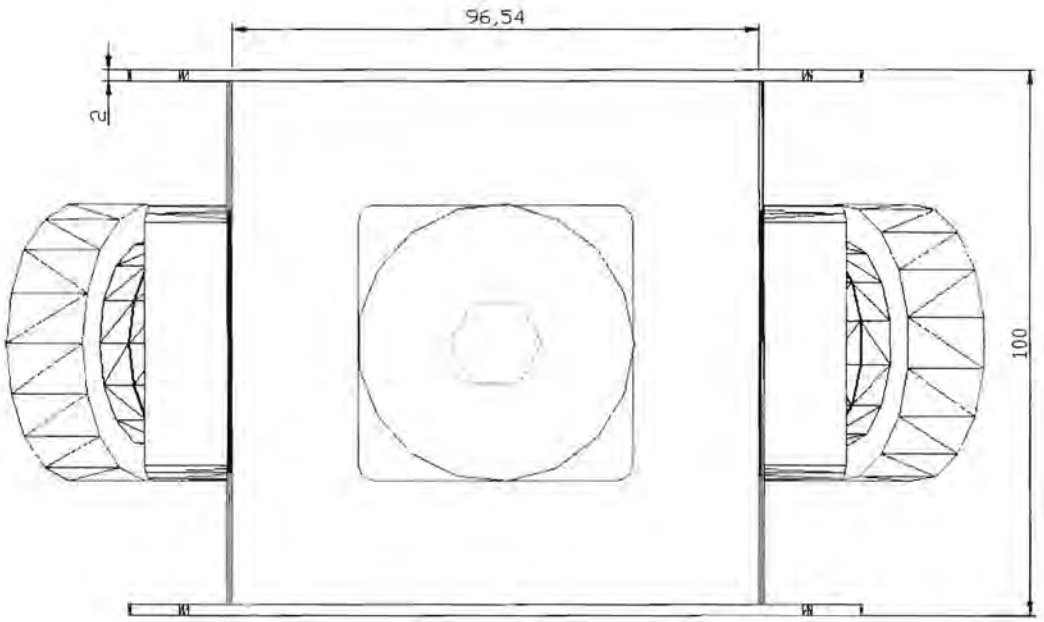
96,54
2
100

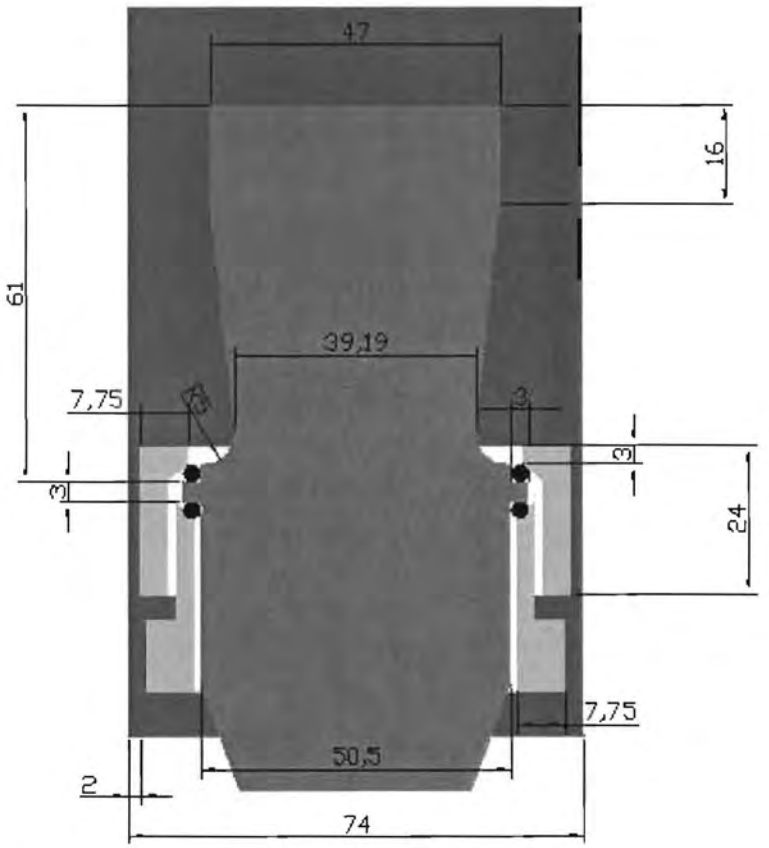
47
16
61
39,19
7,75
3
3
3
24
7,75
50,5
2
74